

OSS (Outer Solar System): A fundamental and planetary physics mission to Neptune, Triton and the Kuiper Belt

B. Christophe · L.J. Spilker ·
J.D. Anderson · N. André ·
S.W. Asmar · J. Aurnou · D. Banfield ·
A. Barucci · O. Bertolami ·
R. Bingham · P. Brown ·
B. Cecconi · J.-M. Courty · H. Dittus ·
L.N. Fletcher · B. Foulon · F. Francisco ·
P.J.S. Gil · K.H. Glassmeier ·
W. Grundy · C. Hansen · J. Helbert ·
R. Helled · H. Hussmann · B. Lamine ·
C. Lämmerzahl · L. Lamy ·
B. Lenoir · A. Levy · G. Orton ·
J. Páramos · J. Poncy · F. Postberg ·
S.V. Progrebenko · K.R. Reh ·
S. Reynaud · C. Robert · E. Samain ·
J. Saur · K.M. Sayanagi · N. Schmitz ·
H. Selig · F. Sohl · T.R. Spilker ·
R. Srama · K. Stephan · P. Touboul ·
P. Wolf

Received: date / Accepted: date

B. Christophe, B. Foulon, B. Lenoir, A. Levy, C. Robert, P. Touboul
ONERA - The French Aerospace Lab, F-92322 Châtillon, France
E-mail: bruno.christophe(at)onera.fr

L.J. Spilker, J.D. Anderson, S.W. Asmar, K.R. Reh, G. Orton, T.R. Spilker
JPL/NASA (USA)

N. André
CESR (France)

D. Banfield
Cornell University (USA)

J. Helbert, H. Hussmann, N. Schmitz, F. Sohl, K. Stephan
DLR/Institute of Planetary Research (Germany)

H. Dittus
DLR/Institute of Space System (Germany)

P. Brown
Imperial College London (UK)

R. Srama

Abstract The present OSS mission continues a long and bright tradition by associating the communities of fundamental physics and planetary sciences in a single mission with ambitious goals in both domains. OSS is an M-class mission to explore the Neptune system almost half a century after flyby of the Voyager 2 spacecraft.

Several discoveries were made by Voyager 2, including the Great Dark Spot (which has now disappeared) and Triton's geysers. Voyager 2 revealed the dynamics of Neptune's atmosphere and found four rings and evidence of ring arcs above Neptune. Benefiting from a greatly improved instrumentation,

IRS, University of Stuttgart and MPIK, Heidelberg (Germany)

F. Francisco, P.J.S. Gil, J. Paramos
Instituto Superior Técnico (Portugal)

S.V. Progrebenko
JIVE, Joint Institute for VLBI in Europe (The Netherlands)

A. Barucci, B. Cecconi, L. Lamy
Laboratoire d'Etudes et d'Instrumentation en Astrophysique, Observatoire de Paris, CNRS, Meudon (France)

J.-M. Courty, B. Lamine, S. Reynaud
LKB, CNRS, Paris (France)

W. Grundy
Lowell Observatory (USA)

E. Samain
Observatoire de la Côte d'Azur, GeoAzur (France)

C. Hansen
PSI (USA)

R. Bingham
RAL (UK)

P. Wolf
SYRTE, Observatoire de Paris-Meudon (France)

J. Poncy
Thales Alenia Space, Cannes (France)

K.H. Glassmeier
Technical University of Braunschweig (Germany)

O. Bertolami
Universidade do Porto (Portugal)

J. Saur
Universität zu Köln (Germany)

J. Aurnou, R. Helled, K.M. Sayanagi
University of California (USA)

F. Postberg
University of Heidelberg (Germany)

L.N. Fletcher
University of Oxford (UK)

C. Lämmerzahl, H. Selig
ZARM, University of Bremen (Germany)

it will result in a striking advance in the study of the farthest planet of the Solar System. Furthermore, OSS will provide a unique opportunity to visit a selected Kuiper Belt object subsequent to the passage of the Neptunian system. It will consolidate the hypothesis of the origin of Triton as a KBO captured by Neptune, and improve our knowledge on the formation of the Solar system.

The probe will embark instruments allowing precise tracking of the probe during cruise. It allows to perform the best controlled experiment for testing, in deep space, the General Relativity, on which is based all the models of Solar system formation.

OSS is proposed as an international cooperation between ESA and NASA, giving the capability for ESA to launch an M-class mission towards the farthest planet of the Solar system, and to a Kuiper Belt object. The proposed mission profile would allow to deliver a 500 kg class spacecraft. The design of the probe is mainly constrained by the deep space gravity test in order to minimise the perturbation of the accelerometer measurement.

Keywords Fundamental Physics · Deep Space Gravity · Neptune · Triton · Kuiper Belt Object

1 Introduction

Gravitational physics and solar system physics have been intimately connected at various stages of their developments. Isaac Newton used the movement of planets as a crucial laboratory for testing his new theory. Pierre-Simon Laplace extended the tools of mathematical physics of gravity and developed the nebular hypothesis of the origin of the Solar System. Urbain Jean Joseph Le Verrier calculated the position of the "eighth planet" by analyzing the perturbations of the orbit of Uranus. Johann Gottfried Galle discovered the new planet, to be later named Neptune, at the predicted position. Le Verrier also analyzed the anomaly of the motion of Mercury which, after a lot of discussions between astronomers and physicists, became the first proof of the validity of general relativity.

The present Outer Solar System Mission (OSS) proposed in the frame of the ESA Cosmic Vision call for a M mission continues this long and bright tradition by associating the communities of fundamental physics and planetary sciences in a mission with ambitious goals in both domains. OSS will visit Neptune and its moon Triton, nearly half a century after Voyager 2. Using a suite of advanced instrumentation with strong European heritage, OSS will provide striking advances in the study of the furthest known planet of the Solar system. The Neptune flyby will be precisely controlled to permit a close encounter with a Kuiper Belt object to be properly chosen among the large number of scientifically interesting and attainable KBOs (this number being much larger than for New Horizons, due to the large mass of Neptune). The mission will consolidate the hypothesis of the origin of Triton as a KBO captured by Neptune at the epoch of formation of the solar system.

During its cruise to the Outer Solar System, the precise tracking of the probe will be used for testing the predictions of General Relativity. The probe will include instruments capable of providing gravitational measurements in deep space, with an accuracy of more than a hundred times better than ever done in the Solar System. Using laser metrology in order to improve the accuracy, the OSS mission will also improve the result of the Cassini spacecraft that performed successfully tested general relativity by measuring Eddington's parameter γ during its interplanetary journey to Saturn.

After a brief description of the scientific objectives of the missions, the instrumentation suite is presented. A brief analysis of the mission profile is performed. Then the spacecraft design is described.

2 Scientific objectives

2.1 Fundamental Physics

2.1.1 Deep space gravity

General Relativity, the current theoretical formulation of gravitation, is in good agreement with most experimental tests of gravitation (Will, 2006). But General Relativity is a classical theory and all attempts to merge it with the quantum description of the other fundamental interactions suggest that it cannot be the final theory of gravitation. Meanwhile, the experimental tests leave open windows for deviations from General Relativity at short (Adelberger et al, 2003) or long distance (Reynaud and Jaekel, 2005) scales.

General Relativity is also challenged by observations at galactic and cosmic scales. The rotation curves of galaxies and the relation between redshifts and luminosities of supernovae deviate from the predictions of the theory. These anomalies are interpreted as revealing the presence of new components of the Universe, the so-called "dark matter" and "dark energy" which are thought to constitute respectively 25% and 70% of the energy content of the Universe (Copeland et al, 2006; Frieman et al, 2008). Their nature remains unknown and, despite their prevalence, they have not been detected by any other means than gravitational measurements. Given the immense challenge posed by these large scale behaviors, it is important to explore every possible explanation including the hypothesis that General Relativity is not a correct description of gravity at large scales (Aguirre et al, 2001; Nojiri and Odintsov, 2007).

Testing gravity at the largest scales reachable by man-made instruments is therefore essential to bridge the gap between experiments in the Solar System and astrophysical or cosmological observations. The most notable existing test in this domain was performed by NASA during the extended Pioneer 10 & 11 missions. This test resulted in what is now known as the Pioneer anomaly (Anderson et al, 1998, 2002), one of the few experimental signals deviating from the predictions of General Relativity (Lämmerzahl et al, 2008; Anderson and Nieto, 2009).

In a context dominated by the quest for the nature of dark matter and dark energy, the challenge raised by the anomalous Pioneer signals has to be faced. Efforts have been devoted to the reanalysis of Pioneer data (Markwardt, 2002; Olsen, 2007; Bertolami et al, 2008; Levy et al, 2009; Turyshev and Toth, 2009)), with the aim of learning as much as possible on its possible origin, which can be an experimental artefact as well as a hint of considerable importance for fundamental physics (Turyshev and Toth, 2010). In the meantime, theoretical studies have been devoted to determine whether or not the anomalous signal could reveal a scale-dependent modification of the law of gravity while remaining compatible with other tests. Among the candidates, one finds metric extensions (Reynaud and Jaekel, 2005; Jaekel and Reynaud, 2005, 2006b,a) as well as field theoretical models (Bertolami and Páramos, 2004; Moffat, 2005, 2006; Brownstein and Moffat, 2006; Bruneton and Esposito-Farèse, 2007; Bertolami et al, 2007) of General Relativity.

Several mission concepts have been put forwards (Anderson et al, 2002; Dittus et al, 2005; Johann et al, 2008; Bertolami et al, 2007; Christophe et al, 2009; Wolf et al, 2009) to improve the experiment performed by Pioneer 10 & 11 probes. A key idea in these proposals is to measure non-gravitational forces acting on the spacecraft, whatever may be the cause of these forces, and thus solve the main ambiguity in the analysis of the Pioneer signal. The addition of an accelerometer on board the spacecraft not only improves the precision and quality of the navigation but also allows for understanding the origin of any anomalous signals. The target accuracy of the accelerometry measurement is 10 pm.s^{-2} . Combining these measurements with radio tracking data, it becomes possible to improve by orders of magnitude the precision of the comparison with theory of the spacecraft gravitational acceleration.

The same instrument also improves the science return with respect to objectives in exploration of the Outer Solar System physics, which is the motivation for combining fundamental physics and planetary physics in a common mission. This idea has been included in the Roadmap for Fundamental Physics in Space issued in 2010 by ESA¹. Let us emphasize at this point that these scientific goals are intimately connected since the law of gravity is directly connected to the planetary ephemeris (Fienga et al, 2010) as well as to the origins of the Solar system (Blanc et al, 2005).

2.1.2 Measurement of the Eddington's parameter γ

The Eddington parameter γ , whose value in general relativity is unity, is a fundamental parameter in most tests of relativistic gravity. In fact, $(1 - \gamma)$ yields one measurement of the deviation from General Relativity from competing theories: it gauges for example, the fractional strength of scalar interaction in scalar-tensor theories of gravity. This deviation $(1 - \gamma)$ has been shown to be smaller than 2×10^{-5} by the Cassini relativity experiment performed at

¹ ESA Fundamental Physics Roadmap Advisory Team, A Roadmap for Fundamental Physics in Space, 2010. Available at [08/23/2010]: <http://sci.esa.int/fprat>

solar conjunctions in June 2002. But recent theoretical proposals suggest that this deviation might have a natural value in the range 10^{-6} - 10^{-7} as a consequence of a damping of the scalar contribution to gravity during cosmological evolution.

The orbit of the spacecraft will be tracked during the whole cruise phase, in order to test General Relativity to an unprecedented level of accuracy (see previous section). A particularly interesting test will take benefit of solar conjunctions to repeat the Cassini relativity experiment, which has given the best constraints on deviations from GR to date. If using the same radio-science as Cassini, the experiment will confirm its results with the advantage of an accelerometer on board to measure the non-geodesic acceleration. A largely improved accuracy can be attained with the up-scaling option of laser ranging equipment onboard. The OSS mission can thus measure the parameter $(1 - \gamma)$ at the 10^{-7} level, which would provide new crucial information on scalar-tensor theories of gravity at their fascinating interface with theories of cosmological evolution.

2.2 Neptune's rings and inner satellites

The OSS science payload and flyby trajectory offer a unique opportunity to increase our understanding of the Neptunian ring system and its retinue of small inner satellites. Ring-moon systems were once perceived as stable and unchanging for time scales of at least 10^6 - 10^8 years. New, higher-quality data from Cassini, Hubble and ground-based telescopes are painting a different picture, in which the systems evolve over years to decades. Cassini images even show changes in the F ring on a scale of hours to days (Murray et al, 2008). The knowledge gained by studying this system of rings and satellites will be applicable to ring systems and planetary disks that occur elsewhere in the universe. Voyager images revealed exquisite complexity and structural variety in ring systems (Smith et al, 1989; Porco et al, 1995). It has the additional scientific interest of being the most remote and least-known ring-moon system in the Solar System and the only other ring system besides Saturn's known to possess relatively stable arcs.

Nicholson et al (1995) extrapolated the arcs' motion backward from the Voyager epoch and showed that all prior occultations were compatible with them, implying longevity of ≥ 5 years (Burns and Cuzzi, 2006). Without a confinement mechanism, arcs should disperse in a matter of weeks. The nearby moon Galatea was quickly recognized as playing a major role in confining the arcs via a corotation resonance (Goldreich et al, 1986; Porco, 1991). However, the Goldreich et al (1986) corotation-sites are in fact unstable when solar radiation forces on dust are taken into account (Foryta and Sicardy, 1996). Thus the dust in the arcs must be replenished by macroscopic source particles. This however poses a new problem, since mutual impacts between macroscopic arc particles will rapidly de-stabilize their confinement (Hanninen and Porco,

1997). In Salo and Hanninen (1998) they show that large particles in corotation sites can be stabilized on non-colliding orbits by their mutual self gravity.

Moreover, such particles could act as a source of dust, and also could confine dust arcs spanning over several co-rotation sites. Observationally one signature would be the clumpy substructure of the arcs due to possible presence of sub-km particles. Several analogues to the Neptune ring arcs have now been found in the Saturn system (Hedman et al, 2007, 2009; Ferrari and Brahic, 1997).

Again, this intensifies the interest in Neptune’s ring arcs for the purpose of comparative studies with the following questions:

1. What is the current configuration of the rings, dust disk, and ring arcs and how has that configuration evolved since the Voyager flyby in 1989?
2. What is the composition of the rings and inner satellites?
3. What are the particle size distributions in the rings and ring arcs? Do larger parent bodies populate and/or confine the ring arcs?
4. What dynamical processes are responsible for ring structure?
5. What is the relationship between the rings and small satellites? Do satellites play a role in confining the ring arcs?
6. Do expansive dust rings exist around Neptune?

2.3 Neptune

Extrasolar planet hunting has matured to the point of not only detecting ice-giant-sized bodies around other stars, but even measuring the bulk compositional properties and mapping out the spatial characteristics and thermal parameters of these extrasolar planets (e.g., Harrington et al (2006)). Our understanding of these extrasolar ice-giants is hampered by our limited knowledge of many basic aspects of our own nearby ice giants, which should serve as templates for their extrasolar cousins.

2.3.1 Neptune Interior

The interior of Neptune is poorly understood but likely composed of a mixture of rock and ices (Hubbard et al, 1991; Podolak et al, 1995). It is not clear, however, if rock and ice components are fully or incompletely separated so that density would increase more gradually toward the centre. The radial extent of the core region could amount up to 70% of the total radius, thereby substantially affecting the planet’s low-degree gravitational field. Unfortunately, however, present-day observational constraints on Neptune’s interior structure are limited to gravitational harmonics to forth degree (J_2 , J_4) within relatively broad error margins. Whereas substantial thermal excess emission implies adiabaticity of Neptune’s deep interior, the presence of a multipolar magnetic field requires electrically conducting fluid regions (probably salty H_2O) at shallow depths (Ness et al, 1989; Stanley and Bloxham, 2004).

Neptune’s shape and rotational state are still imperfectly known to constrain interior structure models (Helled et al, 2010). However, the shape of a

giant planet contains important constraints on its rotation rate, and can be used to discriminate between different rotation profiles (i.e., solid-body rotation vs. differential rotation on cylinders, etc.). The solid-body rotation rate of the planet is required for internal modeling (e.g., Zharkov et al (1978)). In case that the planet rotates differentially, or if the zonal winds are deep enough, the planetary shape is adjusted accordingly, and corrections to the gravitational coefficients and, therefore, the planetary internal structure must be included in the models (Hubbard, 1999; Hubbard et al, 1991). The planetary shape can also be used to constrain the depth of the zonal winds that are crucial for our understanding of magnetic field generation and global circulation in the planet.

Neptune’s Interior Key Scientific Questions and Measurement Objectives:

1. What is the interior structure of Neptune?
2. What is the shape and rotational state of Neptune?
3. Why is Neptune’s internal emitted energy fraction larger than for any other planet in the solar system?

2.3.2 Neptune’s Atmosphere

Neptune has a surprisingly dynamic atmosphere with its great distance from the sun. Even though it receives the weakest solar heating among the atmospheres in our solar system, it has the fastest known jetstream system blowing at almost 500 m/s (Limaye and Sromovsky, 1991). Voyager 2 imaging also revealed the existence of a giant vortex that migrated equatorward and oscillated in a peculiar manner (Smith et al, 1989). How the dynamic weather system of Neptune is powered is largely unknown. Atmospheric aerosols (hazes and clouds in the troposphere and stratosphere) are believed to play a major role in modulating the solar heating when they scatter and absorb incoming radiation, which in turn affects the altitude and temperature of the tropopause and the meridional wind profile; however, the details on how this thermal energy is converted to kinetic energy is yet to be resolved.

In the recent years, observational and modeling studies of jetstreams on Jupiter and Saturn have revealed that small-scale eddies can provide the momentum forcing necessary to drive the jets (e.g., Salyk et al (2006); Del Genio et al (2007); Aurnou et al (2007); Sayanagi et al (2008)). However, although Voyager 2 fly-by and subsequent Earth-based observations have resolved large-scale eddies that vary rapidly (Luszcz-Cook et al, 2010), small eddies that can feed energy and momentum to the larger weather phenomena are yet to be seen on Neptune. The lifecycle and dynamics of the Great Dark Spots is another area that awaits further study. On Jupiter, large vortices grow as a result of vortex mergers (Morales-Juberías et al, 2003). In contrast, the Great Dark Spots on Neptune form in mid-latitudes and then drift equatorward and destroyed when the weak Coriolis effect of the equatorial region can no longer keep a vortex balanced. Even though multiple generations of Great Dark Spots have been observed, smaller scale eddies that may contribute to its maintenance or generation have never been seen, and high-resolution observation

with a camera optimized for probing Neptune will substantially advance our understanding of the dynamic atmosphere.

Neptune’s Atmosphere Key Scientific Questions and Measurement Objectives:

1. How does the atmosphere vary with time at smaller spatial scales, as suggested by Earth-based observations of large-scale changes?
2. What are the atmospheric convection patterns and, if present, zonal circulation patterns at depth in thermal emission? How deep does Neptune’s zonal structure go?
3. What is the tropospheric aerosol composition and particle size in discrete features (Great Dark Spots, bright spots), and how does it differ from the surrounding “unperturbed” atmosphere? What is the aerosol composition and particle size in the stratosphere and upper troposphere?
4. What powers the winds, and why are Neptune’s winds and thermal structure similar to those of Uranus, though the internal heat sources differ?
5. How is Neptune’s energy balance affected by atmospheric temperature?

2.3.3 Neptune’s magnetic field and magnetosphere

Neptune’s magnetic dipole, like that of Uranus, is highly tilted and offset from the planet’s centre (Ness et al, 1989; Ness, 1994; Connerney et al, 1991). The equatorial surface field is $1.42 \mu\text{T}$, corresponding to a magnetic moment about 27 times greater than at Earth. The quadrupole moment of Neptune is quite large and makes a greater contribution to the surface magnetic field than at any other planet, which is symptomatic of a very irregular magnetic field. The octupole and higher moments are essentially undetermined (Connerney et al, 1991). Stanley and Bloxham (2004) have attributed the large tilt and strong quadrupole moment to the thin shell structure and relatively poor electrical conductivity of the ice mantle where the magnetic field is thought to be generated. However, this explanation appears to apply better to Uranus than Neptune where convection may occur throughout the fluid envelope (Fortney et al, 2011).

Because of its unusual orientation and tilt, Neptune’s magnetospheric field goes through dramatic changes as the planet rotates in the solar wind (Bagenal, 1992) with the magnetosphere being completely reconfigured twice per planetary rotation period. Despite this, the Neptunian magnetosphere appeared very quiescent during the Voyager 2 flyby in 1989. The subsolar magnetopause has been observed to lie as far as 26 Neptunian radii in front of the planet. The wave levels and energetic particle fluxes were both very low. Neptune showed no evidence of magnetic substorm activity (Mauk et al, 1995), in spite of the rotationally modulated reconnection with the upstream IMF (Interplanetary Magnetic Field) that must be present. However, in contrast with near-solstice observations of Voyager 2, near-equinox conditions will prevail for approximately 2 decades around 2038. In this configuration, reconnection will be much more favoured once per rotation and will allow one to study the

magnetospheric response to solar wind input on time scales of hours. Such information will reveal how magnetospheres work, and can not be obtained by studying Earth, Jupiter or Saturn alone.

The plasma in Neptune’s magnetosphere is thought to be derived mainly from Triton (Richardson et al, 1991). The N^+ escapes directly from the ionosphere of Triton into Neptune’s magnetosphere, and H^+ is derived from a neutral H torus emanating from Triton. Auroral emissions, associated with energetic electrons circulating along high-latitude magnetic field lines, were unambiguously observed at radio wavelengths (the Neptune’s Kilometric Radiation - NKR - consists of no less than 4 different radio components) around north (N) and south (S) magnetic poles as well as close to the magnetic equator, which is a specificity of ice giants (Zarka et al, 1995). Atmospheric aurorae were also tentatively observed in UV around the S pole (Sandel et al, 1990). A strong confinement of the radiation belts by the minimum L shell of Triton was observed (Mauk et al, 1995); none of these features have been satisfactorily explained.

Magnetic Field and Magnetosphere Key Questions and Measurement Objectives:

1. What is the generation mechanism of Neptunes irregular magnetic field in the low-conductivity convecting interior of Neptune? Is Neptune’s magnetic field subject to secular variations?
2. What is the rotation period of the interior of Neptune?
3. What is the composition of the plasma in Neptunes magnetosphere?
4. What is the nature of the Neptunian solar wind/magnetosphere/ionosphere coupling? Why is Neptune such a complex radio source?
5. What are the operational dynamics of a highly-tilted magnetosphere that refills and empties over diurnal time scales? What is the importance of magnetic reconnection?

2.4 Triton

Triton is likely the only large satellite in the Solar System that did not form in situ around its central planet. Its highly inclined orbit ($\sim 23^\circ$) and retrograde orbit suggests that Triton is a captured dwarf planet from the inner Kuiper Belt. Tidal energy released in the course of orbit circularization should have been sufficient for Triton to differentiate, but there is no measurement of its moment of inertia to be certain. Triton is now locked in a synchronous orbit with nearly the same longitude always facing Neptune (unless there is a slow non-synchronous rotation of an ice shell over a subsurface ocean yet to be detected). Triton’s mass ($2.14 \times 10^{22} kg$) and mean density ($2059 \pm 5 kg/m^3$) (Jacobson, 2009; Thomas, 2000) suggests that the interior is composed of 23% ice and 77% rock (Schubert et al, 2004). Models of the interior favour that Triton is differentiated into a large rocky core with a radius 1062 km and an icy shell of around 290 km depth. However, a good measurement of C_{22} is needed

before any interior model is adopted as most likely. To this end, the interpretation depends on the method of level surfaces, where each ellipsoidal shell has its own shape and density. The level-surface theory for synchronous rotation and tides has been discussed by Hubbard and Anderson (1978), Dermott (1979), and more recently in a series of papers by Zharkov and Gudkova (2010). The application of the theory to a differentiated Triton yields a value for C_{22} of 55.23×10^{-6} . On the other hand if Triton is undifferentiated, with a constant density equal to its mean density, the value of C_{22} is 99.71×10^{-6} , which represents a maximum value. Even if homogeneous in composition, a pressure-induced phase transition from Ice Ih to Ice II deep within Triton would imply a value less than the maximum value.

Since the Voyager encounters, subsurface oceans have been detected in the icy Jovian and is predicted in Enceladus and Titan (Zimmer et al, 2000; Kivelson et al, 2002; Schubert et al, 2007; Lorentz, 2008), as well as in Triton (Stevenson, 2002; Hussmann et al, 2006) indicating that subsurface oceans may be common in icy moons. Determining whether Triton has an ocean, and whether any of its chemistry is expressed on its surface would make Triton an attractive astrobiological target. Subsurface ocean on Triton can be diagnosed particularly well with electromagnetic induction studies since there are two distinct time variable magnetic fields in Triton vicinity. One is due to the highly tilted magnetic field of Neptune and the other one is due to Triton's large inclination. The two field components might allow to resolve the thickness and the conductivity of the ocean separately (Saur et al, 2010).

Voyager returned our first (and only!) closeup Triton data in August 1989 covering only about 40% of its surface with resolution ranging between 60 and 1 km per pixel (Smith et al, 1989). The few highest resolution images show a sparsely cratered young geologically complex surface similar to Europa and Enceladus and landforms of unrevealed origin that are unlike any others seen in our solar system including the "cantaloupe terrain" crisscrossed by quasi-linear ridges similar in appearance to the double ridges on Europa (Prockter et al, 2006) and Enceladus.

Many of Triton's surface features are supposed to be of cryovolcanic origin (Croft et al, 1995), and possibly formed by complex interactions between tidal dissipation, heat transfer, and tectonics that drive the resurfacing on Europa and Enceladus. However, Voyager's limited coverage and spatial resolution prevents us from unraveling Triton's geological history. Numerous dark fans on the bright surface are believed to originate from eruptions no longer active at the time of the Voyager snapshots. Evidence for recent activity was found in Triton's southern polar region where two plumes erupted from the surface during the Voyager flyby (Soderblom et al, 1990), which might be solar-powered, driven by seasonal sublimation and storage of nitrogen under translucent ice, pressurized, then released (Kirk et al, 1990). The model of solar-powered activity has flaws however, including the size of the sub-ice nitrogen reservoir required, and thus the origin of the plumes is still a mystery.

The geology of Triton's 38 K cold surface is as complex as its geology. Triton is covered by various volatile ices (N_2 , CH_4 , H_2O , CO , and CO_2) that sup-

port and interact with a seasonally variable atmosphere (Cruikshank and Apt, 1984; Cruikshank et al, 1984; Conrath et al, 1989; Cruikshank et al, 1991; Grundy et al, 2010) leading to seasonal redistribution of the volatile ices (e.g., Trafton et al (1998)). Triton’s complex seasonal cycle puts Triton in a key position for the understanding of surface-atmosphere interactions on small icy bodies like Pluto and Eris with similar surface volatile inventories (Owen and Encrenaz, 2003; Licandro et al, 2006; Tegler et al, 2008; Abernathy et al, 2009; Merlin et al, 2009).

Radio science observations revealed a significant ionosphere with a well-defined peak at ~ 350 km altitude (Tyler et al, 1989). The distance and the geometry of the Triton closest approach precluded in situ observations of either the ionosphere or its interaction with Neptune’s magnetosphere. Heavy ions, likely associated with Triton’s exosphere were observed to be concentrated towards Neptune’s magnetic equator (Belcher et al, 1989; Richardson et al, 1995).

The outer extent of the high-energy ($\geq \sim 1$ MeV) radiation belt particles at Neptune is set by Triton’s orbit, thought to possibly ”sweep up” these particles as it orbits Neptune (Stone et al, 1989). This behaviour extends to lower energies, but electrons with energies of 10s of keV are present at Triton’s orbit and may be the principal driver for auroral emissions seen by Voyager. Changes in the electron spectral index (~ 20 to 60 keV) peak at Triton’s location are an additional signature of the significant interaction of the moon with Neptune’s magnetosphere at these energies (Krimigis et al, 1989; Mauk et al, 1995).

Triton Key Science Questions and Measurement Objectives are the following:

1. What is the origin and history of Triton’s differentiation? Does Triton have a subsurface ocean? What does the evolution of its interior tell us about the capture process? Does Triton have a current or past dynamo magnetic field?
2. What is the cratering record on Triton and how does it relate to and constrain Solar System formation and early evolution scenarios?
3. How spatially heterogeneous is Triton’s surface? What undiscovered geologic features lie in regions that were not well-imaged by Voyager? How are ices partitioned across the surface? Is Triton presently active?
4. How do volatile inventories compare between Pluto, Triton, and OSS’s in situ KBO? How has seasonal volatile migration affected the south polar cap and atmosphere since Triton has gone from southern spring (Voyager) to summer (OSS)? How much mass has been transferred into the atmosphere and northern polar region?
5. Are Triton’s plumes a result of solar-driven activity? Are the plumes observed by Voyager 2 still erupting, and if so, in the same places or in new areas? What do the sites and timings of occurrence tell us about the energetics, relevant processes, and the nitrogen reservoir?

6. What can we learn about the formation and distribution of aerosols in Triton's atmosphere? How has the wind regime on Triton changed since the Voyager flyby, postsouthern solstice?
7. How is the relatively dense neutral torus of Triton formed, and what is its relationship, if any, to active vents on Triton and/or loss processes from Triton's atmosphere?
8. How does highly conducting Triton interact with the corotating magnetosphere of Neptune? Is this related to the generation and maintenance of Triton's extremely strong ionosphere, which has a peak electron density of $25 \times 10^4 \text{ cm}^{-3}$?

2.5 Kuiper Belt object

Our understanding of the history of our Solar System has been revolutionized, largely because of the discovery of Kuiper Belt Objects (KBOs, Jewitt et al (1992)). Well over a thousand KBOs have since been discovered (e.g. Barucci et al (2008a)), and they exhibit remarkable diversity in their properties. Geometric albedos range from a few percent to nearly 100%, and appear to be correlated with diameter, as well as (possibly) visible color and perihelion distance (Stansberry et al, 2008); cold-classical KBOs appear to be red and have high albedo (Doressoundiram et al, 2008; Brucker et al, 2009). Visible colours span the range from slightly blue to the reddest objects in the Solar System (Pholus). Visible and near-IR spectra run the gamut from profoundly bland to exhibiting absorptions (or emission peaks) due to organics, water, nitrogen, methane and other hydrocarbon ices, and silicates (e.g. Barucci et al (2008b)). Perhaps the most remarkable character of KBOs is the abundance of binary and multiple systems: among the cold-classical KBOs, 30% or more are probably binaries (Noll et al, 2008).

The current number of KBOs, the dynamical structure of their orbits (Kavelaars et al, 2008), and the diverse physical characteristics of the individual objects has spurred intense efforts at modelling the formation and evolution of the KBO population. Beginning with the Malhotra (1993) explanation for Pluto's orbit, these studies have led to a picture in which Saturn crossed through the 2:1 resonance with Jupiter, exciting the orbital eccentricities of Uranus and Neptune, which (as a result) interacted strongly with the primordial Kuiper Belt, suffering significant outward orbital migration.

This scenario explains well the dynamical structure and present-day population of the Kuiper Belt, as well as the origins of the late heavy bombardment in the inner Solar System (Gomes et al, 2005; Morbidelli et al, 2005; Tsiganis et al, 2005; Levison et al, 2008).

This section focuses on KBO science objectives. In many areas, these are very similar to our Triton science objectives. Our overall objective is to guarantee that we obtain the necessary data for detailed comparison of Triton and the OSS KBO to one another, and to Pluto and the New Horizons KBO. Together, these observations will begin to provide significant insights into the

diverse KBO population. In large part, the KBO and Triton sciences objectives drive the OSS science payload.

Particulars of the KBO measurement objectives depend considerably on what target is chosen. It will be very challenging to navigate to close proximity ($0.5r$) of a solitary, small KBO. Its heliocentric orbit will only have been observed for a few decades, and thus will have substantial uncertainties. On-board optical navigation could have a hard time even seeing a smaller KBO from more than a few weeks or months out. This might be another reason to try for a larger one (though it puts more constraints on the Neptune encounter). A binary also helps because its angular separation can be resolved from further away than the disk of a solitary body can be, enabling an earlier refinement of its range. Such an extremely close flyby could also be problematic for surface geology, since there would be very little time to image the surface at the moderate phase angles that bring out surface features. The same goes for phase function and shape/volume determinations.

Because target selection likely will not have been finalized before detailed instrument definition work must be completed, the instruments need to have broad capabilities appropriate for the exploration of primitive bodies in the outer Solar System. Luckily, Triton serves as an excellent proxy to a KBO target, and we do possess some detailed knowledge about a few of the larger KBOs (e.g. spectral features, albedos). Starting with that knowledge, we developed measurement objectives tailored for Triton and the largest KBOs, and then enhanced those to include conditions and objectives appropriate for a range of KBOs (e.g. lower albedo surfaces, more tenuous atmosphere).

Key KBO Science and Measurement Objectives are the following:

1. What can we learn about the bulk and system properties?
2. Is the KBO differentiated, and if so, what are the compositions of various internal layers? Is there a liquid ocean inside the KBO? Is there a remnant magnetic field in the KBO?
3. What can we learn about the geology? What is the cratering record?
4. What is the surface composition?
5. Are volatile ices present, in what quantity, and how are they distributed?
6. Does the KBO retain an atmosphere, and if so, how does it interact with the solar wind?

3 Proposed payload

The strawman instrument payload option as proposed for OSS to address the corresponding scientific objectives and specific questions is presented in Table 1. The mass and consumption of each instrument is given. For the Laser Science Instrument (LSI), the budget doesn't include the USO (LSI-2 ways) or only the additional budget for a better clock (LSI-1 way).

Table 1 OSS strawman instrument payload and corresponding scientific objectives and specific questions as given in Section 2

Instrument Acronym	Scientific Objectives Questions from						Mass (kg)	Power (W)
	§2.1	§2.2	§2.3.1	§2.3.2	§2.3.3	§2.4	§2.5	
ACC	1,2		1			1	2	3.5
RSI	1,2	1	1,2			1,8	1,2	3.0
USO		1	2			8		1.5
VLBI	1,2							-
UVS		1		3	2,3,4,5	3,4	6	5
NIR		2,3		1,3,5	2,4	3,4	4,5	10.1
WAC		6		1,2				7.5
NAC		1-5		4		2,3,5,6	1,3,4	9.8
RPW					2-5			4.7
MAG					1,2,4,5	1	2	3.3
TMI			3	2,4,5		3,4	4	7
DPD		2,3,5,6			3	3,4	4,5	3.5
LSI 2-ways	2							25
LSI 1-way								14.5
								21.5

3.1 ACC - Accelerometer: GAP

The DC accelerometer GAP is used in complement of the navigation instruments (LSI, RSI and/or VLBI) to measure the non gravitational acceleration applied to the spacecraft. It allows to deduce the effect of the gravitational forces on the spacecraft trajectory either for general relativity verification during interplanetary phases either for planet's or moon's gravity field computation during flyby.

GAP is composed of an electrostatic accelerometer MicroSTAR, based on Onera expertise in the field of accelerometry and gravimetry (CHAMP, GRACE, GOCE missions, Touboul et al (1999)), and a bias calibration system. Ready-to-fly technology is used with original improvements aimed at reducing power consumption, size and weight. The bias calibration system consists in a flip mechanism which allows a 180° rotation of the accelerometer to be carried out at regularly spaced times. The flip allows the calibration of the instrument bias along 2 directions, by comparing the acceleration measurement in the two positions Lenoir et al (2010).

The three axes accelerometers are based on the electrostatic levitation of the inertial mass with no mechanical contact with the instrument frame. The proof-mass is then controlled by electrostatic forces and torques generated by six servo loops applying well measured equal voltages on symmetric electrodes. Measurements of the electrostatic forces and torques provide the six outputs of the accelerometer. The mechanical core of the accelerometer is fixed on a sole plate and enclosed in a hermetic housing in order to maintain a good vacuum around the proof-mass (see Figure 1). The electronic boards are implemented around the housing with low consumption analog functions.

The Bias Rejection System is equipped with a rotating actuator and a high-resolution angle encoder working in closed loop operation. The actuator is based on piezo-electric elements which are located inside the ball bearing that

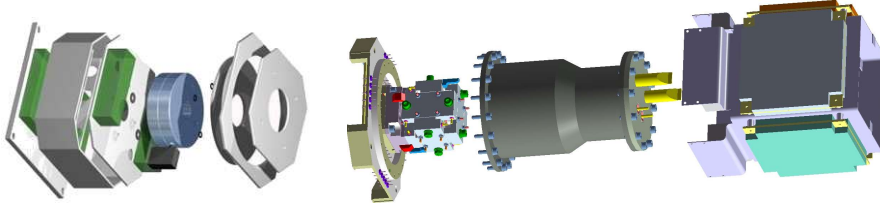


Fig. 1 GAP exploded view: Bias Rejection System (left) and MicroSTAR accelerometer (right)

carries the MicroSTAR SU. The actuator operates in the slip-stick mode which results in a non-zero holding torque in the power-off mode. The electronic boards for driving the piezo actuator and controlling the closed servo loop are located inside the housing. A second small piezo actuator (linear actuator) is foreseen to block the moving part of the rotating actuator during transport and launch.

The Interface and Control Unit (ICU) includes the DC/DC converters and the RS422 serial interface to spacecraft through a FPGA.

The resolution of the instrument is 1 pm/s^2 in DC, with a global performance of 10 pm/s^2 taking into account the effect of integration in the S/C (alignment, centrifugal acceleration, S/C self-gravity ...).

3.2 LSI - Laser Science Instrument

For the verification of the Eddington's parameter γ , it is proposed to use laser Doppler measurement instead of Radio-Science in order to achieve accuracy of 10^{-7} . For this measurement, two different concepts are proposed and briefly described below.

3.2.1 One way Laser - TIPO

The TIPO experiment (Télémétrie Inter Planétaire Optique) proposed by the OCA team is a one-way laser ranging project derived from satellite and lunar laser ranging (SLR/LLR) and optical time transfer T2L2. The TIPO principle is based on the emission of laser pulses from an Earth based station towards the spacecraft. These pulses are timed in the respective timescales at departure on Earth and upon arrival on the spacecraft. The propagation time and the respective distance between Earth and spacecraft are derived from the difference of the dates of departure and arrival. This one-way laser ranging permits distance measurements on a Solar System scale (up to 30 AU) as the one-way link budget varies only with the square of the distance, contrary to the power of four for usual laser telemetry.

The ground segment is a high-fidelity laser ranging station, working solely as an emitter. An example of a suitable ground station is the rejuvenated Ex-LaserLune station "MeO" of OCA in Grasse, France, but there is half

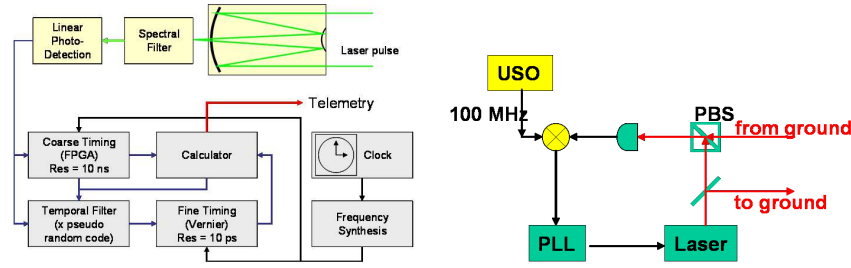


Fig. 2 TIPO (left) and DOLL (right) space segment synopsis

a dozen suitable laser ranging stations worldwide that fully (or with minor enhancement) comply with the requirements (laser power, telescope diameter and pointing performance). These stations will also collaborate for the exploitation of T2L2 from 2008. The space equipment is constituted of an optical subsystem (small telescope and detection device), an electronic subsystem (event timer, detection and control electronics) and a clock (USO - Ultra Stable Oscillator), as sketched in Figure 2 left. The optical subsystem comprises a rather compact telescope in order to collect the incoming laser pulses, a spectral filter for noise reduction and a linear photon detection system with picosecond timing characteristics. Considering maximum distance of 30 AU, a 20 cm aperture telescope and an acquisition phase of 1000 s, the SNR may be raised to a satisfying signal confidence level.

Considering an onboard clock with an Allan variance better than 10^{-15} @ 100 000 s (cold atomic clock HORACE designed by SYRTE or the mercury ion clock designed by JPL), TIPO allows millimetric differential distance measurements over duration of one day. With the JPL ion mercury ion clock (which replaced the USO), the total mass is 16 kg, with 27 W of consumption.

3.2.2 Two way coherent laser - DOLL

The DOLL optical link concept for OSS is the optical equivalent of the radio link, with an on-board laser transponder and ground terminals at already operating satellite/lunar laser ranging stations (Figure 2 right). The optical link is based on the coherent optical link for navigation and timing initially envisaged for SAGAS (Wolf et al, 2009), but is making use of existing flight hardware developed by TESAT GmbH for the Laser Communication Terminal (LCT) presently flying onboard the German TerraSAR-X and the US NFIRE satellites (Gregory et al, 2010). This combines utmost performance with high TRL levels. The OSS-DOLL link adapts ground stations to accommodate most of the changes required for operation over interplanetary distances. In its baseline version OSS-DOLL features in particular:

- Continuous wave laser operation in both directions (two-way system) at $\lambda=1064.5$ nm.

- Heterodyne onboard laser transponder (minor modification of the present homodyne LCT transponder).
- High precision optical Doppler (range-rate) measurement.
- Data transfer and range measurement.
- Large stray light rejection from heterodyne detection and due to a controlled frequency offset (100 MHz) between incoming and outgoing laser signals, using a space qualified USO (ACES/PHARAO Quartz oscillator).

The dominating noise sources in the frequency range of interest are the effects due to the atmosphere (turbulence and slow index variations, the noise model is based on measurement of atmospheric turbulence using optical stellar interferometry (Linfield et al, 2001) and ground links (Djerroud et al, 2010)) and the onboard accelerometer noise at low frequency ($\leq 3 \times 10^{-5}$ Hz), the latter playing only a marginal role in the measurement uncertainty of the Eddington's parameter γ . The resulting overall PSD is $S_y(f) = 10^{-27}/\text{Hz}$ at high frequency, the transition to white phase noise (f^2 slope) at 10^{-3} Hz, and back to white $10^{-27}/\text{Hz}$ white frequency noise at low frequencies from the mm tropospheric model errors.

Thanks to narrow band pass interference filters, the 5 kHz heterodyne detection filter and the reduction by the ratio of "laser spot size" to "Sun spot size", only 5×10^{-16} W of the stray light will arrive to the detector, well below the signal at 10^{-14} W. Moreover, stray light from the outgoing signal into the detection channel is mitigated by using orthogonal polarizations, and by offsetting the outgoing frequency with respect to the incoming one.

The phase coherent detection for DOLL concept requires also adaptive optics methods to ensure phase coherence over the complete aperture of the ground telescope. The effect of turbulence rises if pointing far from Zenith, let say significantly beyond 45° . However the stray light goes up as well, hence limiting the detection of the laser source. Considering day-time standard turbulence conditions and $1.064 \mu\text{m}$ radiations, the Fried's diameter equals 15 cm and the scintillation index is less than 10%, from Zenith to 40° apart. The laser power collected is larger than solar stray light using an aperture diameter of 20 cm and with the previous spectral filtering. Collecting light with a 1.5 m telescope aperture, an adaptive optics correction on the turbulent phase is envisaged. An accurate wavefront measurement is performed across an array of adjacent subapertures of 20 cm in diameter. At the level of the detector of the wavefront sensor, both a pinhole restricting the field of view and a narrow-band-pass filter shall be included to reduce background light. A low order system of correction - typically containing 8×8 subapertures - delivers a more coherent and stable signal, that could feed a heterodyne system of detection with a substantial gain in coherent energy.

The wave-front sensor of the adaptive optics (AO) would use the incoming signal, which requires the development of a low power wave front sensor, operational in the presence of large background light. Such a sensor based on heterodyne interferometry (using a narrow electronic filter to reject stray light) is presently under development at DLR (Oberpfaffenhofen, group of D.

Giggenbach). Another advantage of such a detector is the possibility of using its output directly for the phase measurement, i.e. there is no need to "share" the photons between the AO and science channel.

3.3 RSI - Radio-Science, USO - Ultra-Stable Oscillator and VLBI - Very Large Baseline Interferometer

The Outer Solar System (OSS) Mission has Radio Science objectives in two categories, gravitation and propagation.

The gravitation measurements are based on precision determination of perturbation to the spacecraft motion or orbit as a result of gravitational forces acting on it from planets, moon, rings, or other bodies in its environment as well as relativistic effects. These measurements are made with precision Doppler tracking, which are optimized at two wavelengths, X- and Ka-bands, in a two-way coherent mode. The dual links enable the calibration of the dispersive effects of the charged particles in the interplanetary plasma. X- and Ka-bands have been flown reliably in a coherent mode on at least two deep space missions (Cassini and Juno) and are planned for several more upcoming missions (Bepi-Colombo). The two-way coherent mode enables the transponder(s) to take advantage of the superior stability of H-maser based clocks at the ground stations. A transponder capable of X- and Ka-bands simultaneously is the simplest approach but two transponders with a common link will also achieve the objectives. The performance of the gravitation links can be expressed in Doppler noise in units of velocity or in terms of the dimensionless Allan deviation and should be at least 10^{-14} at an integration time of 1000 s.

The propagation Radio Science experiments measurements are based on precision determination of perturbation in the phase/frequency and amplitude of the radio signals propagating from the spacecraft to Earth by intervening media under study, such as atmospheres and ionospheres of the planets, moons, or other bodies. These measurements are made in the one-way mode utilizing a highly stable reference to generate the signal on-board the spacecraft at two or more links. The dual/multiple one-way links enable the isolation of dispersive material under study such as planetary ionospheres. Numerous deep space missions have successfully utilized this technique for occultation experiments by flying Ultra-Stable Oscillators (USO), which are quartz resonators in single or dual ovens for thermal stabilization. The performance of the propagation links can be expressed in terms of the dimensionless Allan deviation and should be at least 10^{-13} at an integration times between 10 and 1000 s (the current version of USO proposed by University of Köln - an improved version is under study to be part of the Jupiter mission EJSM and to survive in Jupiter hard radiation environment has this stability at 1 s to 100 s and is going to be improved for the Jupiter mission). USOs have very high heritage in deep space with having successfully flown on Voyager, Galileo, Mars Global Surveyor, Cassini, GRACE, Rosetta, Venus Express, and other missions.

Observations of the spacecraft using global VLBI arrays with 10 or more radio telescopes and maximum baselines of $\sim 10\,000$ km at X-band in a phase referencing mode using the natural extragalactic radio sources for phase calibration can provide positioning accuracy at a level of 0.1 nrad, or 150 m at a distance of 10 AU. Regarding the on-board segment, no special requirements on top of the Radio Science and USO are implied. VLBI can be done on the regular transmission signals provided a power in the data carrier line and ranging tones (combined) will be a level of 1 W at 20 dBi TX antenna gain, ranging tones separation of ~ 100 MHz and intrinsic frequency stability at a level of 10^{-12} at 100 s. VLBI observations of the signals transmitted during the two-way link Radio Science experiments will improve the Doppler measurements by a factor of 1.4 due to the averaging of the propagation scintillations effects in Earth troposphere, ionosphere and interplanetary plasma.

3.4 NAC - High resolution Narrow Angle Camera

The High Resolution Camera will conduct imaging science of multiple targets of interests in the Neptunian system. It will be used to measure global cloud motions during the approach phase of the mission, map the fine-scale structure of its ring system, and make high-resolution global surface map of Triton. High resolution (colour) and panchromatic imagery of the Neptunian system is envisaged with 0.005 mrad spatial resolution. The optics will be designed as a reflective telescope with a large focal length and an imaging array sensor, which can be operated either in a pushbroom mode for high resolution panchromatic imaging of Triton during flyby (with flyby involved motion compensation for enabling long exposures) or in a conventional framing mode (for high resolution and color images of the Neptunian system and to obtain images to support spacecraft tracking).

The instrument will consist essentially of 3 components, the optics, the sensor system, and a data processing unit. The optics will be a reflecting telescope involving a primary mirror and a secondary convex mirror. The focal length is 3 m. The baseline sensor is a CMOS Star1000 1024 x 1024 array sensor (pixel size $15\ \mu\text{m}$), which is known to be radiation-resistant, and for which much heritage is available. Optionally, a motorized filter wheel with 12 filter positions could be mounted in front of the entrance optics to allow for colour and multispectral observations of distant targets in the Neptunian system.

The instrument will operate during the tour through the Neptunian system as well the KBO observations. The pointing prediction shall be sufficiently accurate to successfully point the camera at distant targets. The pointing shall be stable within the size of $1/3$ image pixel during the typical exposure time of 0.5 s. During orbit, the camera shall maintain nadir-pointing. The direction of the motion vector must be held throughout the orbit mission. The instrument operation schedule should allow for geometric and radiometric calibration, instrument alignment cross-calibration and performance tests. The calibration

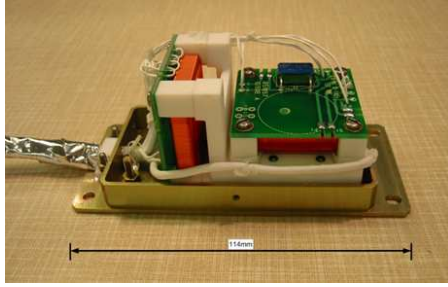


Fig. 3 Double Star fluxgate sensor

is done by measurements of instrument alignment with the spacecraft coordinate system using star observations and radiometric calibration of the camera using star observations.

The performance characteristics of the instrument are:

- Spectral range: 350 - 1050 nm;
- Field of view: 0.293° ;
- Pixel field of view: 0.005 mrad

3.5 MAG - Magnetometer

The magnetometer will measure the magnetic field vector in the bandwidth DC to 128 Hz, depending on precise science requirements and available telemetry. The magnetometer consists of at least one but preferably two tri-axial fluxgate sensors, which would be boom mounted in order to minimise magnetic interference (less than a few nT), and a platform mounted electronics box.

Two sensors are preferred to facilitate operation as a gradiometer in order to separate the very small target ambient field changes from any magnetic disturbance field due to the probe fields. The sensors would be ring core fluxgates, similar to that shown in Figure 3 which would draw on considerable space heritage (TRL 8/9).

Fluxgate sensors can feature very low noise ($\leq 10pT/\sqrt{Hz}$) above 1 Hz, good offset stability ($\leq 0.05nT/K$) and scale factor drift ($\leq 40ppm/K$).

The fluxgate is implemented within the standard feedback loop (housed on the electronics card) featuring bipolar driving of the soft magnetic ring core and second harmonic detection of the field proportional feedback voltage. The sensor electronics would be a digital FPGA based design (direct heritage from Solar Orbiter and THEMIS), or an ASIC which would require further specific development but offer a reduction in instrument power consumption.

The magnetometer has no pointing or active alignment requirements; however accurate knowledge of the sensor orientation (to better than 0.1°) is required in order to accurately determine the field direction. The magnetometer would be calibrated on the ground prior to launch. In-flight calibration will

determine the spacecraft induced field, verify the extent to which the ground calibration remains valid and to quantify changes in calibration parameters.

Fluxgate magnetometers have considerable heritage on orbiting spacecraft including Ulysses, Cassini, Double Star, Rosetta, Venus Express, and THEMIS (e.g. Carr et al (2005); Glassmeier et al (2007)). One issue with the fluxgate sensor is the cold environment at the outer planets in the event that no power resource is available for MAG sensor heating. It is predicted that the temperature in the environment of boom mounted sensor in Neptune orbit could be as low as 70 K. There are currently technology studies underway into cold running of fluxgates as part of EJSM instrument studies.

3.6 RPW - Radio and Plasma Wave

The RPW experiment will provide remote and in situ measurements of radio and plasma wave phenomena in the frequency range from a fraction of a Hz up to about 20-40 MHz for electric fields and 100 kHz for magnetic fields. The scientific objectives of this experiment are (i) the determination of the Poynting vector and the full polarization state of electromagnetic waves for remote sensing of Neptunian (NKR) and heliospheric electromagnetic emissions, (ii) a high frequency coverage up to 20-40 MHz to sample a significant portion of the spectrum of NEDs (Neptunian Electrostatic Discharge), whose low frequency cut-off would provide a remote sensing tool of the sub-spacecraft electron peak ionospheric density and (iii) the detailed study of local wave phenomena and the identification of characteristic frequencies of the local plasma. This experiment is based on a very strong European heritage corresponding to a high TRL.

RPW will include three 5-m long electric orthogonal monopole antennas and three magnetic orthogonal search coils. After pre-amplification, the sensors outputs are processed by a low-frequency receiver from 0 to 20 kHz including a waveform sampler, and a high-frequency receiver from 10 kHz to 20 MHz able to measure auto- and cross-correlations of signals simultaneously sensed on two channels, stored in an electronic box. The experiment is powered by DC/DC converter and controlled by a central microprocessor (DPU) which will be used in flight to reconfigure the sensor outputs and to maximize the science return with respect to available bit rate and power.

Such an experiment has a high TRL with strong space heritage (Cassini/RPWS, STEREO/Waves and ongoing developments for Solar Orbiter/RPWI, Bepi-Colombo MMO/RPW/Sorbet and EJSM/RPWI).

The RPW instrument is very versatile and can operate in many modes with various time and frequency sampling characteristics. There will be onboard processing; either for onboard key parameter computation, for event triggering, or for lossless compression. Based on Cassini/RPWS, the typical telemetry rate is a few kbps.

RPW electric and magnetic sensors are sensitive to electric and magnetic interferences. While the radio antenna will be fixed directly on the spacecraft

body, magnetic search coils need to be placed on a boom, that can be that of the magnetometer. Several calibration procedures will be conducted: ground-based calibrations of the receiving chain, ground based calibration of sensors and in-flight calibration (with internal or external known sources).

3.7 NIR - Near infrared imager and WAC - wide angle camera: NORTON

NORTON will be used to image Neptune during the closest approach to capture the detailed global view of atmospheric cloud structure while simultaneously resolving the small eddy and aerosol structures using multiple filters. This instrument is heavily based on the RALPH subsystem of the New Horizons mission (Reuter et al, 2008), and inherits much of the architecture and technology of that instrument system with modifications to the detector and filter systems. The very similar performance demands on the New Horizons spacecraft to those of the OSS mission result in a convergent evolution with the Near-IR mapping spectrometer sharing optics with the wide-angle imaging camera. This results in a considerable mass savings, as the telescopes are a significant mass of an imaging instrument, especially for the low illumination and longer flyby distances in the outer solar system.

NORTON shares the same optical design as RALPH, a single highly baffled 75 mm aperture in front of an f/8.7 visible/near-IR off-axis three-mirror telescope. This design provides good thermal and alignment stability, and adequate light throughput. Stray light is controlled not only via baffling, but also a Lyot stop at the exit pupil and further baffling at an intermediate focus. At the end of the telescope a dichroic beamsplitter delivers the light from wavelengths longer than $1.1\ \mu\text{m}$ to the Near-IR focal plane while shorter wavelengths are sent to the visible focal plane.

The visible focal plane is almost identical to the MVIC sub-instrument from New Horizon's RALPH, with 9 independent 5024×32 CCD arrays operated in time delay integration (TDI) mode. Two of those arrays are used to produce panchromatic imagery (400-975 nm) while the other 7 are combined with filters to produce images in discrete bandpasses, blue (400-500 nm), green (500-600 nm), red (600-700 nm), near-IR (700-975 nm) and a narrow band methane (860-910 nm) and two nearby continuum channels (810-860 nm and 910-960 nm). The angular resolution of each pixel in the visible focal plane is $20 \times 20\ \mu\text{radian}^2$, and the static FOV of the TDI array is $5.7^\circ \times 0.037^\circ$, the same as RALPH's MVIC. For targets like Neptune or Triton, NORTON's visible focal plane will yield images with a signal to noise higher than 48 for all bandpasses.

The near-IR focal plane is also quite similar to the LEISA sub-instrument from New Horizon's RALPH, but with somewhat more extensive modifications. In particular, while the RALPH's LEISA instrument was sensitive from $1.25\text{-}2.5\ \mu\text{m}$, NORTON's near-infrared focal plane will cover $1.25\text{-}4.5\ \mu\text{m}$. Additionally, technology now allows a much larger HgCdTe detector array (2048×2048 H2RG) to be used. The near-IR focal plane uses a linear variable

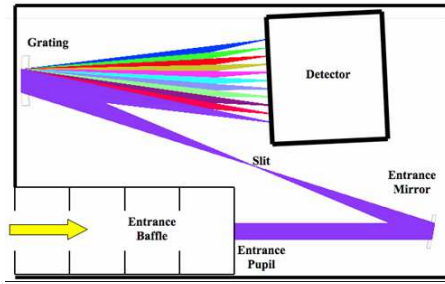


Fig. 4 Optical concept of the UV spectrometer

filter superimposed on top of the detector to limit different columns of the detector array to be sensitive to different wavelengths. As the instrument is scanned past a scene, a particular region of the scene illuminates pixels sensitive to different wavelengths, thus building up a spectral image cube of the whole scene. NORTON's near-IR spectral resolution will be $R=600$ throughout its bandpass, with a spatial resolution of $50 \times 50 \mu\text{radian}^2$, and a FOV width of 5.87° . The SNR of NORTON's near-IR focal plane for a target such as Neptune will yield a measurement of the reflectivity with a signal to noise ratio of about 30 throughout the bandpass.

3.8 UVS - Ultraviolet imaging spectrometer: UVIS

The instrument measures photons in the 55-155 nm range with a spectral resolution of 0.54 nm (fwhm). The spatial resolution is 0.05° , with a temporal resolution of 1s. The sensitivity is 0.47 count:s/R for extended source. The instrument can measure emissions from the atmosphere of Neptune and Triton, either nadir observations or airglow emissions of the upper atmosphere. Vertical sounding of major species can be obtained by stellar occultation's (wavelength, species).

The instrument is a grating spectrometer, composed of a collecting part and a detector part. The collecting part is composed of an entrance baffle, a primary off-axis mirror and a slit. The detector part is composed of a grating and an intensified detector. The intensifier uses a CsI photocathode and a Micro-Channel Plate in front of Cross-Delay Resistive Anode Detector. The Spacecraft interface is handled by a local DPU. The optical concept is shown in Figure 4.

Stellar occultations are performed by pointing the platform in a chosen direction and staying in inertial pointing for a few minutes. Other observations can be done either in inertial mode or in nadir pointing mode. The required pointing accuracy is half the slit width (0.05°) with a stability of 0.05° during the integration time (1 s). In inertial mode, the platform should be stable within one slit width (360 arc sec) over a few minutes (for occultations).

A first calibration is performed on the ground. Evolution of the instrument sensitivity is measured in-flight by looking at stars. Some manoeuvres, such as rolls, are required to perform in-flight checks on straylight levels and polarization characterization. The CsI photocathode must be kept in vacuum. The detector unit has a window which is opened once after launch. For ground activities, the window can be opened when in a vacuum tank. When the window is closed, the detector is pumped on a regular basis to maintain a sufficient vacuum level.

The instrument has heritage from various existing or in-development instruments: PHEBUS on BepiColombo, SPICAM-UV channel on Mars-Express and SPICAV-UV on Venus-Express.

3.9 TMI - Thermal imager OPTIS

OPTIS is a thermal infrared imaging spectrometer with an integrated radiometer. The scientific goal of OPTIS is to provide detailed information about the mineralogical composition of an solid surfaces in the outer solar system by measuring the spectral emittance in the spectral range from 7-12 μm with a high spatial and spectral resolution. Furthermore OPTIS will obtain radiometric measurements in the spectral range from 7-40 μm to study the thermophysical properties.

OPTIS builds on the heritage of the MERTIS instrument for the ESA Bepi-Colombo mission to Mercury. MERTIS is using an uncooled microbolometer array as detector for the spectrometer, to minimize the need for cooling in the hot environment around Mercury. OPTIS instead uses a cooled MCT array detector to maximize the signal to noise ratio for the much colder surface of Triton and KBO. OPTIS has a FOV of 11.7° giving a much larger coverage of the surface within one orbit. Depending on the mission scenario OPTIS can be adapted to a smaller FOV.

The spectrometer of OPTIS is based on the Offner design with a micro-machined grating. In combination with the MCT detector OPTIS will cover the spectral range from 7-12 μm with a spectral resolution of 200nm and a high spatial resolution. The radiometer is highly miniaturized and integrated in the slit plane of the spectrometer. The approach of combining a spectrometer and a radiometer with the same entrance optics provides synergies benefiting the scientific analysis. The fact that the surface temperature can be obtained independently from the spectral measurements allows removing ambiguities in the retrieval of emissivity values. The radiometer will further map thermal physical properties like thermal inertia, texture and grain size.

The instrument design is driven by a strong need for miniaturisation and a modular combination of the functional units at the same time. The complexity of internal interfaces requires a permeate design functionally consisting out of the Sensor Head and the Electronics Unit with the pointing/calibration units in front of the optical entrance. The sensor head structure contains the entrance and spectrometer optics, the bolometer and radiometer focal plates,

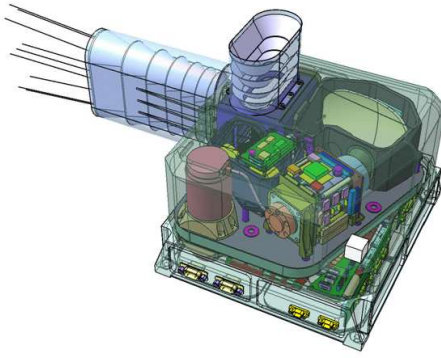


Fig. 5 Concept views of OPTIS (view inside the instrument)

its proximity electronics, the calibration devices (shutter and 300 K black body) and provides thermal interfaces to the Spacecraft to achieve required high thermal stability (Figure 5). At its optical entrance a pointing device is located which directs the incoming infrared beam from 4 different targets, 3 for in-flight calibration purposes and the planet view itself: planetary body view, the look into deep space (space view), the image of the 300 K black body and the image of a spectral calibration target.

OPTIS will typically operating in a mapping mode. In this mode the instrument will alternate between the three calibration views and the planet view with a defined duty cycle. Spectral and radiometric data are obtained simultaneously. Binning in spectral as well as spatial direction can be performed in the instrument by software mode to optimize the signal to noise ratio based on the temperature of the target.

3.10 Dust Particle Detector

The in-situ dust sensor is based upon impact ionization and measures size, speed, direction, and chemical composition of individual dust grains. An interplanetary spacecraft to Neptune provides the unique possibility to link inner solar system dust (processed) with outer solar system dust (Kuiper belt particles) properties. Furthermore, Neptune's variable dusty ring system is of particular interest and its properties like extension, density, variability, and composition shall be studied and compared to the Jovian and Saturnian ring systems, which have been studied by similar dust detectors. At a close flyby the detector encounters material lifted up from Triton's surface by micro meteoroid bombardment. It thus offers the unique opportunity of compositional in situ studies of Triton surface. The novel dust telescope, a successor of the instruments flown aboard Stardust, Galileo and Cassini can operate during cruise and encounter phases.

The instrument measures low dust fluxes (interplanetary micrometeoroid background) as well as high impact rates e.g., when crossing ring segments.

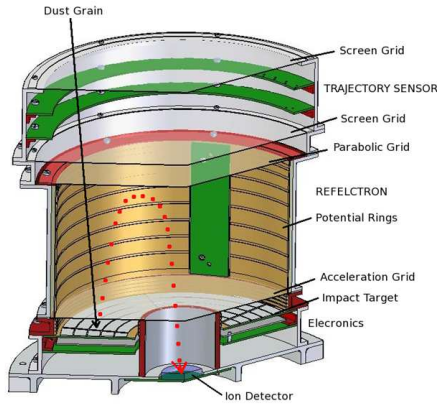


Fig. 6 Dust Detector Particle Instrument

Therefore the dust instrument package operates in two modes: the cruise mode and the encounter mode. The cruise mode is optimised to measure low dust fluxes down to $\sim 10^{-4} \text{ m}^2/\text{s}$, small particle sizes ($\geq 10\text{-}15 \text{ g}$), high impact speeds ($\geq 2 - 50 \text{ km/s}$), grain primary charge ($\geq 0.5 \text{ fC}$) and the particle composition of individual dust grains. The encounter mode provides reliable information about the dust environment with its high fluxes. In order to achieve this wide range of measurement parameters, the instrument packages combines impact ionisation, TOF spectrometry and charge induction as detection methods. A basis of this multi-coincidence detector is a small dust telescope using ring shaped target segments. A plane of charge sensitive wires at the instrument aperture measures grain primary charges, whereas the impact is triggered by the grain hitting a target segment (Figure 6). The integrated Sensor package has a field-of-view of $\pm 40^\circ$.

The TRL is 5/9 due to the heritage of former Stardust (CIDA) and Cassini (CDA) instrumentation.

4 Mission Profile and spacecraft design

The capability to embark the instrument suite defined in the previous chapter is highly dependent on the chosen orbit and launcher. The following section presents a preliminary analysis of the mission profile showing the capability to deliver a 500 kg class probe. Then the design of the spacecraft is briefly described with the main characteristics required either by the science goals or by the mission profile.

4.1 Mission Profile

The selected orbit shall meet the following criteria:

1. Long ballistic periods to follow geodesic arcs to as large a heliocentric distance as possible for gravity measurements,
2. Sun occultation for Eddington parameter measurement,
3. Neptune and Triton flybys for planetary science measurements, then a flyby of a scientifically selected Kuiper Belt object,
4. Transfer to Neptune in less than 13 years,
5. Mission ΔV , and thus the onboard propellant quantity, as small as possible to increase the delivered mass,
6. Low Departure velocity (C3) to reduce launch cost.

The first requirement is naturally achieved by Neptune objective, leading to heliocentric distance larger than 30 AU, with possible extension after Neptune flyby.

For the second requirement, as Neptune's orbit is not in the ecliptic plane, the Earth-Sun-spacecraft conjunctions can occur only early in the mission or when the spacecraft is near the ecliptic plane. With direct transfers, two conjunctions will occur, at 2.1 AU (6 months after departure) and at 4.3 AU. An indirect transfer increases the number of solar conjunction during inner solar system trajectory.

The Neptune encounter provides access to a huge cone of trans-Neptunian space in order to achieve the third requirement. The amount of trajectory bending that can be achieved varies with the V_∞ of approach to Neptune and the trajectory's minimum distance from Neptune. For an approach V_∞ of 10 km/s and minimum distance of 4000 km above the 1-bar level in the atmosphere, that angle is very close to 90° . Faster and farther decrease the angle; slower could increase it. Trajectory modelling shows that tens of known KBOs are accessible to OSS, and the flyby geometry can be tailored to not only achieve science goals within the Neptune system, but continue on to a scientifically-selected Kuiper Belt Object afterward (Marley and et al, 2010).

For the last requirements different strategies have been analysed. A direct trajectory would enable almost annual launch windows at the expense of a relatively heavy launcher due to the high initial velocity required. Transfers using inner solar system gravity assists would allow less heavy launchers. Two optimized trajectories are compared in Figure 7.

Table 2 gives the main characteristics of the different orbit strategies and the delivered mass to Neptune transfer orbit. V_∞ corresponds to Neptune arrival. For the direct launch, Star48 propulsion module is required. The ΔV presented doesn't take into orbit control which required a minimal ΔV of 120 m/s (50 m/s for the launch window, 30 m/s for the launcher dispersion correction, 30 m/s for trajectory correction during cruise and 10 m/s for planet approach), leading to 34 kg of mono-propellant and inert mass for a spacecraft of 500 kg.

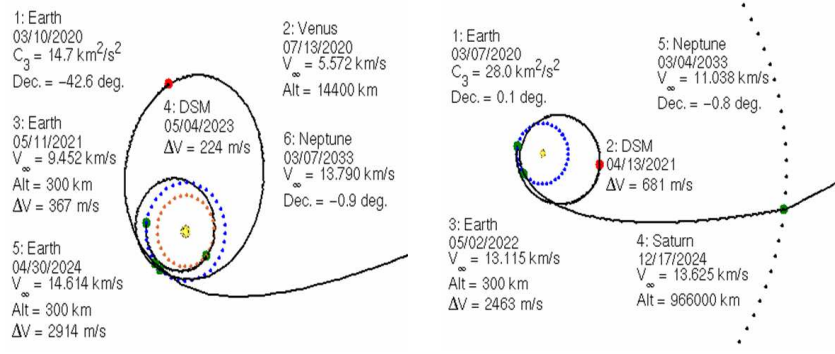


Fig. 7 OSS orbit for a launch in 2020, with Venus and Earth flybys - VEEGA (left) and Earth and Saturn flybys - EESN (right)

Table 2 Orbit characteristics and delivered mass (kg) on Neptune transfer orbit

Orbit	C_3 (km^2/s^2)	ΔV (m/s)	V_∞ (km/s)	Propellant Isp (s)	Soyuz Fregat	Atlas 401	Atlas 551
Direct	159.5	-	8.48	-	-	-	500
VEEGA	14.7	3505	13.79	320	351	845	1594
				220	211	509	961
EESN	28.0	3144	11.04	320	258	713	1402
				220	164	452	890

4.2 Spacecraft

The spacecraft design is based on the hypothesis of a direct launch, with 34 kg of propellant for orbit control. In case of indirect launch, the additional ΔV required will have an impact on the size of the tank, or required a specific propulsion module.

The spacecraft architecture illustrated in Figure 8 and 9 and is organized so as to:

- Provide a planet-pointing side with the observation instruments
- Accommodate the RPW and the dust analyzer properly wrt velocity vector
- Accommodate the MAG with an adequate boom
- Accommodate the laser instrument for the measurement of the Eddington parameter with a pointing towards the Earth
- Provide the lowest and most axisymmetrical gravitational field as viewed from GAP
- Make coincide as much as possible the dry mass centre of gravity, the propellant centre of gravity, the radiation pressure force line and the GAP
- Ensure a stable and reliable alignment between the GAP and the HGA to ensure consistency between radio science and accelerometry
- Accommodate the two ASRGs required for the mission by minimising their impact on the rest of the spacecraft (including radiation)

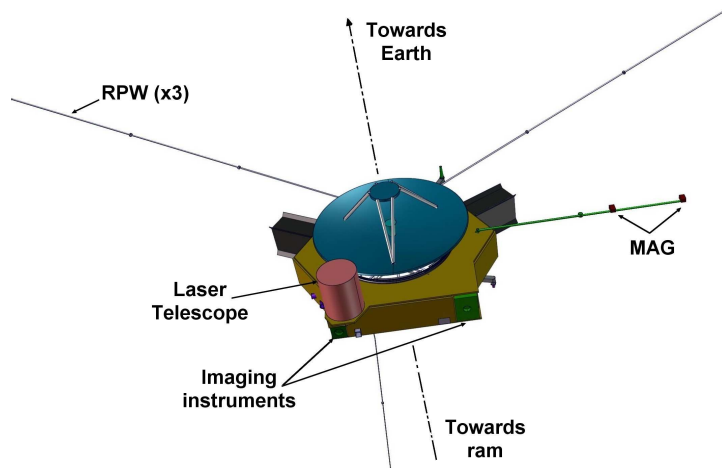


Fig. 8 Spacecraft as viewed from the terminator of the planetary object: accommodating the dust analyzer on the ram face and the RPW and the MAG on large booms protects their measurements from disturbances; the laser, which will have measured the Eddington parameter when closer to the Sun, has its boresight aligned with the HGA

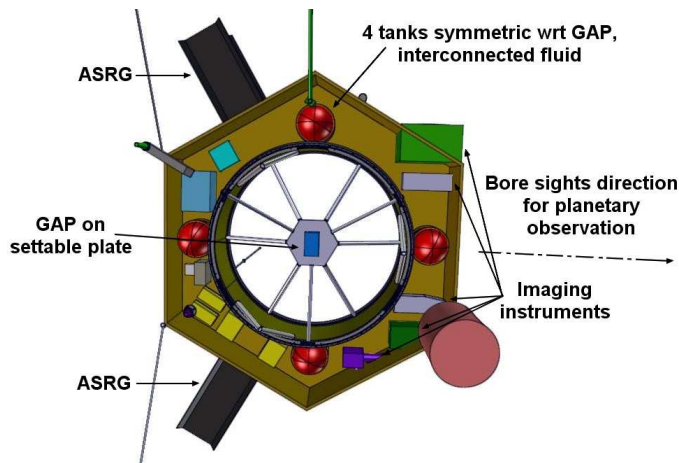


Fig. 9 Spacecraft viewed from top, with HGA and closure panels removed: The New Horizons-like planetary science payload accommodation ensures the planetary science objective while the distribution of the matter on a ring favours the accuracy of the measurements by the GAP.

To this end the platform is built as a flat ring, exterior to a 1666 mm tube, easily interfaceable with Atlas 5, with the New-Horizons-like HGA on top, the GAP accelerometer at the centre of the tube and at the CoG. The GAP is on a settable plate at the centre, held by thermally stable struts. Platform units are accommodated so as to balance the CoG.

The four Hydrazine tanks, a monopropellant with Isp (220 s), are distributed symmetrically far from the GAP, with fluidic interconnection to bal-

ance the quantity of propellant. The knowledge of the propellant location is ensured by the membrane. In addition, a gauging method is proposed to limit the uncertainty on the quantity of propellant. The best compromise is a mix between book keeping offering a good precision at beginning of using and thermal gauging offering good performance at the end. From preliminary computation, the self-gravity uncertainty could be limited to 4 pm/s² along the antenna axis and 14 pm/s² along the transversal axis.

The two ASRGs are accommodated so that their radiators cannot couple with each other and the radiation they emit can be efficiently screened before it reaches the other units of the spacecraft. ASRG is a new type of RPS, and it is still being developed. It uses a Stirling engine (with moving parts) to convert thermal energy to electricity with better efficiency than thermocouples. As a result, ASRGs produce more electricity than MMRTGs, even though they require only one-fourth as much ²³⁸Pu. The output power is 146 Wel at the begin of lifetime and drops to 125 Wel after 14 years.

The upper face is generally pointed toward the Sun and Earth, hosting the HGA and the laser telescope. The downlink data rate will be similar to the one of New Horizons, but with the advantage of the Ka-band. With 70 m ground antenna, a data rate of 1 kbits/s could be achieved at a distance of 36 AU. Considering data size of 5 Gbits after compression as for New Horizons, 172 days are required to download the data using a session length of 8 hours per day. A storage is considered to store safely all the data before their transmission.

The lower face (launcher interface) is generally pointed towards the ram, bearing the dust analyzer and perpendicular to one of the three RPW. One lateral "face" is pointable towards the planetary surfaces with all imaging instruments boresights in that direction.

Two modes are foreseen for the spacecraft: 3-axis stabilized mode during measurement and a spin-mode during the hibernation. The 3-axis stabilization allows high pointing accuracy during the entire measurement period. This mode is controlled by star trackers and gyro-stellar filter system and commanded by reaction wheels. The reaction wheels are desaturated with hydrazine thrusters. The same thrusters are used for re-orientation of the spacecraft or for switching in spin mode. During hibernation, the attitude control will switch to a spin stabilized Earth pointing mode, with an angular rate around 5 rpm, in order to limit ground operations and safe components lifetime on board.

The guidance and control system is capable of providing spin axis attitude knowledge of the spacecraft to better than $\pm 0.027^\circ$ (3σ) and spin phase angle knowledge within $\pm 0.30^\circ$ (3σ). The same knowledge is provided for all axes when the spacecraft is in 3-axis stabilised mode.

A specific analysis has been done for the deep space gravity test. This test occurs during the interplanetary cruise with a global pointing accuracy requested of 1 mrad ($\pm 0.06^\circ$) of the accelerometer measurement axes with the inertial reference frame axes. This misalignment shall be shared between several contributors. An accuracy of 0.5 mrad ($\pm 0.03^\circ$) is allocated for the space-

Table 3 OSS preliminary mass budget

	Estimate in kg
Structure	68
Thermal Control	21
Mechanisms	9
Communications	35
Data Handling	17
AOCS	31
Propulsion	16
Power	86
Harness	24
Instruments	48
Propellant	34
Total mass estimate	389
Plus maturity margins	450
Plus system margin 20%	540

craft pointing in accordance with its performance. During the deep space gravity measurement, the wheels unloading must be avoided: thrusters can't avoid parasitic motions of the probe, saturating the accelerometer. Fortunately, in deep space, disruptive constant torque loading the wheels mainly comes from the solar flux pressure which is low far away and which acts if the probe is not axisymmetric around its sun axis. Far from the sun it can be noticed that the sun - probe - earth angle is very small implying that the 2.1 m HGA is quasi pointed toward the sun offering a frontal circular surface to the sun avoiding torque. Implementing classical 12 Nms RWS must allow avoiding unloading operation during more than one month.

For the elaboration of the OSS concept a conservative margin philosophy has been applied that reflects the early stage of the design. For the mass budget (see Table 3), a system level mass margin of 20% of the dry mass is applied. At equipment level, design maturity mass margins have been applied as per ESA's rules. A margin of 10% is applied on propellant for trajectory manoeuvres and a margin of 100% is applied on propellant for attitude control. The propellant budget is assessed at 34 kg, taking into account only the interplanetary cruise. The total mass is 540 kg, with 48 kg of payload.

The power is sized assuming two ASRGs, with an EOL capacity of 125 useful Watts each, hence 250 W of available power resource, which is comparable to that of the New Horizons spacecraft. Given the higher payload consumption, the power subsystem is complemented by a 25 kg battery, recharged outside of fly-bys and of communication periods. The battery supplies the complement needed during fly-bys so as to allow the simultaneous operation of all instruments and radioscience. This complement of 2400 W.h at 70% of depth of discharge will allow an increase of 100 W in the resources over a period of 24 h, so from 8 h before Triton fly-by to about 8 h after Neptune fly-by.

With respect to classical outer planet flyby mission, the specificity of OSS

is the deep space gravity test which occurs during the interplanetary phase where the spacecraft is nominally in hibernation mode. The deep space measurement will occur several times by year (in order to detect deviation of the general relativity at 0.5 or 1 year) and some long period of one month (in order to detect variation of the general relativity at 0.5 or 1 sidereal day). During this measurement, the spacecraft shall go out the hibernation mode. JPL DSN station with Ka transmitter shall be used to achieve the accuracy of orbit determination. VLBI is also an option to improve this orbit determination. Better will be the accuracy of positioning, shorter could be the measurement period.

Acknowledgements This proposal was supported by CNES (France) through a phase 0 study managed by E. Hinglais.

OSS scientific team thanks Argo scientific team who accepts for this proposition to use their white papers for Decadal Survey (Spilker and Argo Team, 2010; Hansen and Argo Team, 2010a,b; Stansberry and Argo Team, 2010).

References

- Abernathy M, Tegler S, Grundy W, Licandro J, Romanishin W, Cornelison D, F V (2009) Digging into the surface of the icy dwarf planet Eris. *Icarus* 199(2):520–525
- Adelberger E, et al (2003) Tests of the Gravitational Inverse-Square Law. *Annual Review of Nuclear and Particle Science* 53:77–121
- Aguirre A, Burgess C, Friedland A, Nolte D (2001) Astrophysical constraints on modifying gravity at large distances. *Class Quantum Grav* 18(R223)
- Anderson J, Nieto M (2009) Astrometric solar-system anomalies. *Proceedings of the International Astronomical Union* 5:189–197
- Anderson JD, Laing PA, Lau EL, Liu AS, Nieto MM, Turyshev SG (1998) Indication, from pioneer 10/11, galileo, and ulysses data, of an apparent anomalous, weak, long-range acceleration. *Phys Rev Lett* 81(14):2858–2861, DOI 10.1103/PhysRevLett.81.2858
- Anderson JD, Laing PA, Lau EL, Liu AS, Nieto MM, Turyshev SG (2002) Study of the anomalous acceleration of pioneer 10 and 11. *Phys Rev D* 65(8):082,004, DOI 10.1103/PhysRevD.65.082004
- Aurnou J, Heimpel M, Wicht J (2007) The effects of vigorous mixing in a convective model of zonal flow on the ice giants. *Icarus* 190:110–126, DOI 10.1016/j.icarus.2007.02.024
- Bagenal F (1992) Giant planet magnetospheres. *Annu Rev Earth Planet Sci* 20:289–328
- Barucci MA, Boehnhardt H, Cruikshank DP, Morbidelli A (2008a) The Solar System Beyond Neptune: Overview and Perspectives, pp 3–10
- Barucci MA, Brown ME, Emery JP, Merlin F (2008b) Composition and Surface Properties of Transneptunian Objects and Centaurs, pp 143–160
- Belcher JW, et al (1989) Plasma Observations Near Neptune: Initial Results from Voyager 2. *Science* 246(4936):1478–1482

- Bertolami O, Páramos J (2004) The Pioneer anomaly in the context of the braneworld scenario. *Classical and Quantum Gravity* 21(13):3309–3321
- Bertolami O, Böhmer CG, Harko T, Lobo FSN (2007) Extra force in $f(r)$ modified theories of gravity. *Phys Rev D* 75(10):104,016, DOI 10.1103/PhysRevD.75.104016
- Bertolami O, Francisco F, Gil PJS, Páramos J (2008) Thermal analysis of the pioneer anomaly: A method to estimate radiative momentum transfer. *Phys Rev D* 78(10):103,001, DOI 10.1103/PhysRevD.78.103001
- Blanc M, et al (2005) Tracing the Origins of the Solar System. *ESLAB Symposium Proceedings*, ESA Special Publications 588:213–224
- Brownstein J, Moffat J (2006) Gravitational solution to the Pioneer 10/11 anomaly. *Class Quantum Gravity* 23(10):3427
- Brucker M, Grundy W, Stansberry J, Spencer J, Sheppard S, Chiang E, Buie M (2009) High albedos of low inclination Classical Kuiper belt objects. *Icarus* 201(1):284–294
- Bruneton JP, Esposito-Farèse G (2007) Field-theoretical formulations of mond-like gravity. *Phys Rev D* 76(12):124,012, DOI 10.1103/PhysRevD.76.124012
- Burns JA, Cuzzi JN (2006) Our Local Astrophysical Laboratory. *Science* 312(5781):1753–1755
- Carr C, Brown P, Zhang TL, Gloag J, Horbury T, Lucek E, Magnes W, O’Brien H, Oddy T, Auster U, Austin P, Aydogar O, Balogh A, Baumjohann W, Beek T, Eichelberger H, Fornacon K, Georgescu E, Glassmeier K, Ludlam M, Nakamura R, Richter I (2005) The Double Star magnetic field investigation: instrument design, performance and highlights of the first year’s observations. *Annales Geophysicae* 23:2713–2732, DOI 10.5194/angeo-23-2713-2005
- Christophe B, Andersen PH, Anderson JD, Asmar S, Bério P, Bertolami O, Bingham R, Bondu F, Bouyer P, Bremer S, Courty J, Dittus H, Foulon B, Gil P, Johann U, Jordan JF, Kent B, Lämmerzahl C, Lévy A, Métris G, Olsen O, Páramos J, Prestage JD, Progrebenko SV, Rasel E, Rathke A, Reynaud S, Rievers B, Samain E, Sumner TJ, Theil S, Touboul P, Turyshev S, Vrancken P, Wolf P, Yu N (2009) Odyssey: a solar system mission. *Experimental Astronomy* 23:529–547, DOI 10.1007/s10686-008-9084-y, [arXiv:0711.2007\[gr-qc\]](https://arxiv.org/abs/0711.2007)
- Connerney JEP, Acuna MH, Ness NF (1991) The magnetic field of Neptune. *Journal of Geophysical Research* 96:19,023–+
- Conrath B, Flasar FM, Hanel R, Kunde V, Maguire W, Pearl J, Pirraglia J, Samuelson R, Cruikshank D, Horn L (1989) Infrared observations of the Neptunian system. *Science* 246:1454–1459, DOI 10.1126/science.246.4936.1454
- Copeland E, Sami M, Tsujikawas S (2006) Dynamics of dark energy. *Int J Mod Phys D* 15(11):1753–1935
- Croft SK, Kargel JS, Kirk RL, Moore JM, Schenk PM, Strom RG (1995) The geology of Triton. In: D P Cruikshank, M S Matthews, & A M Schumann (ed) *Neptune and Triton*, pp 879–947

- Cruikshank DP, Apt J (1984) Methane on Triton - Physical state and distribution. *Icarus* 58:306–311, DOI 10.1016/0019-1035(84)90047-2
- Cruikshank DP, Brown RH, Clark RN (1984) Nitrogen on Triton. *Icarus* 58:293–305, DOI 10.1016/0019-1035(84)90046-0
- Cruikshank DP, Owen TC, Geballe TR, Schmitt B, de Bergh C, Maillard J, Lutz BL, Brown RH (1991) Tentative Detection of CO and CO₂ Ices on Triton. In: *Bulletin of the American Astronomical Society, Bulletin of the American Astronomical Society*, vol 23, pp 1208–+
- Del Genio AD, Barbara JM, Ferrier J, Ingersoll AP, West RA, Vasavada AR, Spitale J, Porco CC (2007) Saturn eddy momentum fluxes and convection: First estimates from Cassini images. *Icarus* 189:479–492, DOI 10.1016/j.icarus.2007.02.013
- Dermott SF (1979) Shapes and gravitational moments of satellites and asteroids. *Icarus* 37:575–586, DOI 10.1016/0019-1035(79)90015-0
- Dittus H, Turyshv S, Lämmerzahl C, Theil, Förstner R, Johann U, Ertmer W, Rasel E, Dachwald B, Seboldt W, Hehl F, Kiefer C, Blome HJ, Kunz J, Giulini D, Bingham R, Kent B, Sumner T, Bertolami O, Pramos J, Christophe B, Foulon B, Touboul P, Bouyer P, Reynaud S, Brillet A, Bondu F, Samain E, de Matos C, Erd C, Grenouilleau J, Izzo D, Rathke A, Anderson J, Asmar S, Lau E, Nieto M, Mashoon B (2005) A Mission to Explore the Pioneer Anomaly. ESA Special Publications 588:3–10, [arXiv:gr-qc/0506139](#)
- Djerroud K, Acef O, Clairon A, Lemonde P, Man CN, Samain E, Wolf P (2010) Coherent optical link through the turbulent atmosphere. *Optics Letters* 35:1479–+, DOI 10.1364/OL.35.001479, [arXiv:0911.4506\[physics.optics\]](#)
- Doressoundiram A, et al (2008) , pp 91–104
- Ferrari C, Brahic A (1997) Arcs and clumps in the Encke division of Saturn’s rings. *Planetary and Space Science* 45:1051–1067, DOI 10.1016/S0032-0633(97)00059-7
- Fienga A, Laskar J, Kuchynka P, Le Poncin-Lafitte C, Manche H, Gastineau M (2010) Gravity tests with INPOP planetary ephemerides. In: *IAU Symposium, Relativity in Fundamental Astronomy: Dynamics, Reference Frames, and Data Analysis*, vol 261, pp 159–169
- Fortney JJ, Ikoma M, Nettelmann N, Guillot T, Marley MS (2011) Self-consistent Model Atmospheres and the Cooling of the Solar System’s Giant Planets. *The Astrophysical Journal* 729:32–+, DOI 10.1088/0004-637X/729/1/32, [arXiv:1101.0606\[astro-ph.EP\]](#)
- Foryta DW, Sicardy B (1996) The Dynamics of the Neptunian ADAMS Ring’s Arcs. *Icarus* 123:129–167, DOI 10.1006/icar.1996.0146
- Frieman JA, et al (2008) Dark Energy and the Accelerating Universe. *Annual Review of Astronomy and Astrophysics* 46:385
- Glassmeier K, Richter I, Diedrich A, Musmann G, Auster U, Motschmann U, Balogh A, Carr C, Cupido E, Coates A, Rother M, Schwingenschuh K, Szegö K, Tsurutani B (2007) RPC-MAG The Fluxgate Magnetometer in the ROSETTA Plasma Consortium. *Space Science Review* 128:649–670,

- DOI 10.1007/s11214-006-9114-x
- Goldreich P, Tremaine S, Borderies N (1986) Towards a theory for Neptune's arc rings. *Astronomical Journal* 92:490494
- Gomes R, Levison HF, Tsiganis K, Morbidelli A (2005) Origin of the cataclysmic Late Heavy Bombardment period of the terrestrial planets. *Nature* 435:466–469, DOI 10.1038/nature03676
- Gregory M, et al (2010) TESAT Laser Communication Terminal Performance Results in 5.6 GBit Coherent Inter-satellite and Satelliteto-Ground links. Proc Int Conf on Space Optics, session 8a [Http://www.icsoproceedings.org/](http://www.icsoproceedings.org/)
- Grundy WM, Young LA, Stansberry JA, Buie MW, Olkin CB, Young EF (2010) Near-infrared spectral monitoring of Triton with IRTF/SpeX II: Spatial distribution and evolution of ices. *Icarus* 205:594–604, DOI 10.1016/j.icarus.2009.08.005, [arXiv:0908.2623\[astro-ph.EP\]](#)
- Hanninen J, Porco C (1997) Collisional Simulations of Neptune's Ring Arcs. *Icarus* 126:1–27, DOI 10.1006/icar.1996.5613
- Hansen C, Argo Team (2010a) Neptune Science with Argo A Voyage through the Outer Solar System. Decadal Survey white paper
- Hansen C, Argo Team (2010b) Triton Science with Argo A Voyage through the Outer Solar System. Decadal Survey white paper
- Harrington J, Hansen BM, Luszcz SH, Seager S, Deming D, Menou K, Cho J, Richardson LJ (2006) The Phase-Dependent Infrared Brightness of the Extrasolar Planet γ Andromedae b. *Science* 314:623–626, DOI 10.1126/science.1133904, [arXiv:astro-ph/0610491](#)
- Hedman MM, Burns JA, Tiscareno MS, Porco CC, Jones GH, Roussos E, Krupp N, Paranicas C, Kempf S (2007) The Source of Saturn's G Ring. *Science* 317:653–, DOI 10.1126/science.1143964
- Hedman MM, Murray CD, Cooper NJ, Tiscareno MS, Beurle K, Evans MW, Burns JA (2009) Three tenuous rings/arcs for three tiny moons. *Icarus* 199:378–386, DOI 10.1016/j.icarus.2008.11.001
- Helled R, Anderson JD, Schubert G (2010) Uranus and Neptune: Shape and rotation. *Icarus* 210:446–454, DOI 10.1016/j.icarus.2010.06.037, [arXiv:1006.3840\[astro-ph.EP\]](#)
- Hubbard WB (1999) NOTE: Gravitational Signature of Jupiter's Deep Zonal Flows. *Icarus* 137:357–359, DOI 10.1006/icar.1998.6064
- Hubbard WB, Anderson JD (1978) Possible flyby measurements of Galilean satellite interior structure. *Icarus* 33:336–341, DOI 10.1016/0019-1035(78)90153-7
- Hubbard WB, Nellis WJ, Mitchell AC, Holmes NC, McCandless PC, Limaye SS (1991) Interior structure of Neptune - Comparison with Uranus. *Science* 253:648–651, DOI 10.1126/science.253.5020.648
- Husmann H, Sohl F, Spohn T (2006) Subsurface oceans and deep interiors of medium-sized outer planet satellites and large trans-neptunian objects. *Icarus* 185:258–273, DOI 10.1016/j.icarus.2006.06.005
- Jacobson R (2009) The Orbits of the Neptunian Satellites and the Orientation of the Pole of Neptune. *The Astronomical Journal* 137:4322–4329, DOI 10.1088/0004-6256/137/5/4322

-
- Jaekel M, Reynaud S (2005) Post-Einsteinian tests of linearized gravitation. *Classical and Quantum Gravity* 22:2135–2157, DOI 10.1088/0264-9381/22/11/015, [arXiv:gr-qc/0502007](#)
- Jaekel M, Reynaud S (2006a) Post-Einsteinian tests of gravitation. *Classical and Quantum Gravity* 23:777–798, DOI 10.1088/0264-9381/23/3/015, [arXiv:gr-qc/0510068](#)
- Jaekel M, Reynaud S (2006b) Radar ranging and Doppler tracking in post-Einsteinian metric theories of gravity. *Classical and Quantum Gravity* 23:7561–7579, DOI 10.1088/0264-9381/23/24/025, [arXiv:gr-qc/0610155](#)
- Jewitt D, Luu J, Marsden BG (1992) 1992 QB1. *IAU circ* 5611:1–+
- Johann U, Dittus H, Lämmerzahl C (2008) Exploring the Pioneer Anomaly: Concept Considerations for a Deep-Space Gravity Probe Based on Laser-Controlled Free-Flying Reference Masses. In: H Dittus, C Lämmerzahl, and SG Turyshev (ed) *Lasers, Clocks and Drag-Free Control: Exploration of Relativistic Gravity in Space, Astrophysics and Space Science Library*, vol 349, pp 577–+, DOI 10.1007/978-3-540-34377-6\26
- Kavelaars J, Jones L, Gladman B, Parker JW, Petit J (2008) The Orbital and Spatial Distribution of the Kuiper Belt, pp 59–69
- Kirk RL, Soderblom LA, Brown RH (1990) Subsurface energy storage and transport for solar-powered geysers on Triton. *Science* 250:424–429, DOI 10.1126/science.250.4979.424
- Kivelson MG, Khurana KK, Volwerk M (2002) The Permanent and Inductive Magnetic Moments of Ganymede. *Icarus* 157:507–522, DOI 10.1006/icar.2002.6834
- Krimigis SM, Bostrom CO, Cheng AF, Armstrong TP, Axford WI (1989) Hot plasma and energetic particles in Neptune’s magnetosphere. *Science* 246:1483–1489, DOI 10.1126/science.246.4936.1483
- Lämmerzahl C, Preuss O, Dittus H (2008) Is the Physics Within the Solar System Really Understood? In: H Dittus, C Lämmerzahl, and S G Turyshev (ed) *Lasers, Clocks and Drag-Free Control: Exploration of Relativistic Gravity in Space, Astrophysics and Space Science Library*, vol 349, pp 75–101, DOI 10.1007/978-3-540-34377-6\3
- Lenoir B, Levy A, Foulon B, Christophe B, Lamine B, Reynaud S (2010) Electrostatic accelerometer with bias rejection for Gravitation and Solar System physics. *ArXiv e-prints Submitted to Advances in Space Research*, [arXiv:1011.6263\[physics.ins-det\]](#)
- Levison HF, Morbidelli A, Vanlaerhoven C, Gomes R, Tsiganis K (2008) Origin of the structure of the Kuiper belt during a dynamical instability in the orbits of Uranus and Neptune. *Icarus* 196:258–273, DOI 10.1016/j.icarus.2007.11.035, [arXiv:0712.0553\[astro-ph\]](#)
- Levy A, Christophe B, Bério P, Métris G, Courty J, Reynaud S (2009) Pioneer 10 Doppler data analysis: Disentangling periodic and secular anomalies. *Advances in Space Research* 43:1538–1544, DOI 10.1016/j.asr.2009.01.003, [arXiv:0809.2682\[gr-qc\]](#)
- Licandro J, Pinilla-Alonso N, Pedani M, Oliva E, Tozzi GP, Grundy WM (2006) The methane ice rich surface of large TNO 2005 FY₉: a Pluto-twin in

- the trans-neptunian belt? *Astronomy and Astrophysics* 445:L35–L38, DOI 10.1051/0004-6361:200500219
- Limaye SS, Sromovsky LA (1991) Winds of Neptune - Voyager observations of cloud motions. *Journal of Geophysical Research* 96:18,941–+
- Linfield RP, Colavita MM, Lane BF (2001) Atmospheric Turbulence Measurements with the Palomar Testbed Interferometer. *The Astrophysical Journal* 554:505–513, DOI 10.1086/321372, [arXiv:astro-ph/0102052](#)
- Lorentz (2008)
- Luszcz-Cook SH, de Pater I, Ádámkovics M, Hammel HB (2010) Seeing double at Neptune’s south pole. *Icarus* 208:938–944, DOI 10.1016/j.icarus.2010.03.007, [arXiv:1003.3240\[astro-ph.EP\]](#)
- Malhotra R (1993) The origin of Pluto’s peculiar orbit. *Nature* 365:819–821, DOI 10.1038/365819a0
- Markwardt CB (2002) Independent Confirmation of the Pioneer 10 Anomalous Acceleration. *ArXiv General Relativity and Quantum Cosmology e-prints* [arXiv:gr-qc/0208046](#)
- Marley M, et al (2010) JPL Rapid Mission Architecture Neptune-Triton-KBO Study Final Report. Planetary Science Decadal Survey
- Mauk BH, Krimigis SM, Cheng AF, Selesnick RS (1995) Energetic particles and hot plasmas of Neptune. In: D P Cruikshank, M S Matthews, & A M Schumann (ed) *Neptune and Triton*, pp 169–232
- Merlin F, Alvarez-Candal A, Delsanti A, Fornasier S, Barucci MA, DeMeo FE, de Bergh C, Doressoundiram A, Quirico E, Schmitt B (2009) Stratification of Methane Ice on Eris’ Surface. *The Astronomical Journal* 137:315–328, DOI 10.1088/0004-6256/137/1/315
- Moffat JW (2005) Gravitational theory, galaxy rotation curves and cosmology without dark matter. *Journal of Cosmology and Astroparticle Physics* 5:3–+, DOI 10.1088/1475-7516/2005/05/003, [arXiv:astro-ph/0412195](#)
- Moffat JW (2006) Scalar tensor vector gravity theory. *Journal of Cosmology and Astroparticle Physics* 3:4–+, DOI 10.1088/1475-7516/2006/03/004, [arXiv:gr-qc/0506021](#)
- Morales-Juberías R, Sánchez-Lavega A, Dowling TE (2003) EPIC simulations of the merger of Jupiter’s White Ovals BE and FA: altitude-dependent behavior. *Icarus* 166:63–74, DOI 10.1016/S0019-1035(03)00259-8
- Morbidelli A, Levison HF, Tsiganis K, Gomes R (2005) Chaotic capture of Jupiter’s Trojan asteroids in the early Solar System. *Nature* 435:462–465, DOI 10.1038/nature03540
- Murray CD, Beurle K, Cooper NJ, Evans MW, Williams GA, Charnoz S (2008) The determination of the structure of Saturn’s F ring by nearby moonlets. *Nature* 453:739–744, DOI 10.1038/nature06999
- Ness NF (1994) Intrinsic Magnetic Fields of the Planets: Mercury to Neptune. *Royal Society of London Philosophical Transactions Series A* 349:249–260, DOI 10.1098/rsta.1994.0129
- Ness NF, Acuna MH, Burlaga LF, Connerney JEP, Lepping RP (1989) Magnetic fields at Neptune. *Science* 246:1473–1478

- Nicholson PD, Mosqueira I, Matthews K (1995) Stellar occultation observations of Neptune's rings: 1984-1988. *Icarus* 113:295–330, DOI 10.1006/icar.1995.1025
- Nojiri S, Odintsov S (2007) Introduction to modified gravity and gravitational alternative for dark energy. *International Journal of Geometric Methods in Modern Physics* 4(1):115–145
- Noll KS, Grundy WM, Chiang EI, Margot JL, Kern SD (2008) , pp 345–36
- Olsen Ø (2007) The constancy of the Pioneer anomalous acceleration. *Astronomy and Astrophysics* 463:393–397, DOI 10.1051/0004-6361:20065906
- Owen T, Encrenaz T (2003) Element Abundances and Isotope Ratios in the Giant Planets and Titan. *Space science reviews* 106:121–138, DOI 10.1023/A:1024633603624
- Podolak M, Weizman A, Marley M (1995) Comparative models of Uranus and Neptune. *Planetary and Space Science* 43:1517–1522, DOI 10.1016/0032-0633(95)00061-5
- Porco CC (1991) An explanation for Neptune's ring arcs. *Science* 253:995–1001, DOI 10.1126/science.253.5023.995
- Porco CC, Nicholson PD, Cuzzi JN, Lissauer JJ, Esposito LW (1995) Neptune's ring system. In: D P Cruikshank, M S Matthews, & A M Schumann (ed) *Neptune and Triton*, pp 703–804
- Prockter LM, Rivkin AS, McNutt RL Jr, Gold RE, Ostdiek PH, Leary JC, Fiehler DI, Oleson SR, Witzberger KE (2006) Enabling Decadal Survey Science Goals for Primitive Bodies Using Radioisotope Electric Propulsion. In: S Mackwell & E Stansbery (ed) *37th Annual Lunar and Planetary Science Conference, Lunar and Planetary Inst. Technical Report*, vol 37, pp 1922–+
- Reuter DC, Stern SA, Scherrer J, Jennings DE, Baer JW, Hanley J, Hardaway L, Lunsford A, McMuldroy S, Moore J, Olkin C, Parizek R, Reitsma H, Sabatke D, Spencer J, Stone J, Throop H, van Cleve J, Weigle GE, Young LA (2008) Ralph: A Visible/Infrared Imager for the New Horizons Pluto/Kuiper Belt Mission. *Space Sci Rev* 140:129–154, DOI 10.1007/s11214-008-9375-7, [arXiv:0709.4281\[astro-ph\]](#)
- Reynaud S, Jaekel MT (2005) Testing the Newton law at long distances. *International Journal of Modern Physics A* 20:2294, DOI 10.1142/S0217751X05024523
- Richardson JD, Belcher JW, Zhang M, McNutt RL Jr (1991) Low-energy ions near Neptune. *J Geophys Res* 96:18,993–+
- Richardson JD, Belcher JW, Szabo A, McNutt RL Jr (1995) The plasma environment of Neptune. In: D P Cruikshank, M S Matthews, & A M Schumann (ed) *Neptune and Triton*, pp 279–340
- Salo H, Hanninen J (1998) Neptune's Partial Rings: Action of Galatea on Self-Gravitating Arc Particles. *Science* 282:1102–+, DOI 10.1126/science.282.5391.1102
- Salyk C, Ingersoll AP, Lorre J, Vasavada A, Del Genio AD (2006) Interaction between eddies and mean flow in Jupiter's atmosphere: Analysis of Cassini imaging data. *Icarus* 185:430–442, DOI 10.1016/j.icarus.2006.08.007

- Sandel BR, Herbert F, Dessler AJ, Hill TW (1990) Aurora and airglow on the night side of Neptune. *Geophysical Research Letters* 17:1693–1696, DOI 10.1029/GL017i010p01693
- Saur J, Neubauer FM, Glassmeier K (2010) Induced Magnetic Fields in Solar System Bodies. *Space Science Rev* 152:391–421, DOI 10.1007/s11214-009-9581-y
- Sayanagi KM, Showman AP, Dowling TE (2008) The Emergence of Multiple Robust Zonal Jets from Freely Evolving, Three-Dimensional Stratified Geostrophic Turbulence with Applications to Jupiter. *Journal of Atmospheric Sciences* 65:3947–1962, DOI 10.1175/2008JAS2558.1
- Schubert G, Anderson JD, Spohn T, McKinnon WB (2004) Interior composition, structure and dynamics of the Galilean satellites, pp 281–306
- Schubert G, Anderson JD, Travis BJ, Palguta J (2007) Enceladus: Present internal structure and differentiation by early and long-term radiogenic heating. *Icarus* 188:345–355, DOI 10.1016/j.icarus.2006.12.012
- Smith BA, Soderblom LA, Banfield D, Barnet C, Beebe RF, Bazilevskii AT, Bollinger K, Boyce JM, Briggs GA, Brahic A (1989) Voyager 2 at Neptune - Imaging science results. *Science* 246:1422–1449, DOI 10.1126/science.246.4936.1422
- Soderblom LA, Becker TL, Kieffer SW, Brown RH, Hansen CJ, Johnson TV (1990) Triton's geyser-like plumes - Discovery and basic characterization. *Science* 250:410–415, DOI 10.1126/science.250.4979.410
- Spilker L, Argo Team (2010) Neptune Ring Science with Argo A Voyage through the Outer Solar System. Decadal Survey white paper
- Stanley S, Bloxham J (2004) Convective-region geometry as the cause of Uranus' and Neptune's unusual magnetic fields. *Nature* 428:151–153, DOI 10.1038/nature02376
- Stansberry J, Argo Team (2010) KBO Science with Argo A Voyage through the Outer Solar System. Decadal Survey white paper
- Stansberry J, Grundy W, Brown M (2008) Physical Properties of Kuiper Belt Objects and Centaurs: Spitzer Space Telescope Constraints. In: Barucci, M A, Boehnhardt, H, Cruikshank, D P, Morbidelli, A, & Dotson, R (ed) *The Solar System Beyond Neptune*, pp 161–179
- Stevenson D (2002) Planetary oceans. *Sky Telesc* 104:38–44
- Stone EC, Cummings AC, Looper MD, Selesnick RS, Lal N, McDonald FB, Trainor JH (1989) Energetic charged particles in the magnetosphere of Neptune. *Science* 246:1489–1494, DOI 10.1126/science.246.4936.1489
- Tegler SC, Abernathy MR, Grundy WM, Romanishin W, Cornelison D, Vilas F (2008) Digging Into the Surface of the Icy Dwarf Planet Eris. In: AAS/Division for Planetary Sciences Meeting Abstracts #40, *Bulletin of the American Astronomical Society*, vol 40, pp 462–+
- Thomas P (2000) The Shape of Triton from Limb Profiles. *Icarus* 148:587–588, DOI 10.1006/icar.2000.6511
- Touboul P, Willemenot E, Foulon B, Josselin V (1999) Accelerometers for CHAMP, GRACE and GOCE space missions: synergy and evolution. In: *Joint Meeting of the International Gravity Commission and the Interna-*

- tional Geoid Commission No2, *Bollettino di Geofisica Teorica ed Applicata*, vol 40, pp 321–327
- Trafton LM, Matson DL, Stansberry JA (1998) Surface/atmosphere Interactions and Volatile Transport (triton, Pluto and Io). In: B Schmitt, C de Bergh, & M Festou (ed) *Solar System Ices, Astrophysics and Space Science Library*, vol 227, pp 773–+
- Tsiganis K, Gomes R, Morbidelli A, Levison HF (2005) Origin of the orbital architecture of the giant planets of the Solar System. *Nature* 435:459–461, DOI 10.1038/nature03539
- Turyshv SG, Toth VT (2009) The Pioneer Anomaly in the Light of New Data. *Space science reviews* 148:149–167, DOI 10.1007/s11214-009-9543-4, [arXiv:0906.0399\[gr-qc\]](#)
- Turyshv SG, Toth VT (2010) The Pioneer Anomaly. *Living Reviews in Relativity* 13:4–+, [arXiv:1001.3686\[gr-qc\]](#)
- Tyler GL, Sweetnam DN, Anderson JD, Borutzki SE, Campbell JK, Kursinski ER, Levy GS, Lindal GF, Lyons JR, Wood GE (1989) Voyager radio science observations of Neptune and Triton. *Science* 246:1466–1473, DOI 10.1126/science.246.4936.1466
- Will CM (2006) The confrontation between general relativity and experiment. *Living Reviews in Relativity* 9(3), URL <http://www.livingreviews.org/lrr-2006-3>
- Wolf P, Bordé CJ, Clairon A, Duchayne L, Landragin A, Lemonde P, Santarelli G, Ertmer W, Rasel E, Cataliotti FS, Inguscio M, Tino GM, Gill P, Klein H, Reynaud S, Salomon C, Peik E, Bertolami O, Gil P, Páramos J, Jentsch C, Johann U, Rathke A, Bouyer P, Cacciapuoti L, Izzo D, de Natale P, Christophe B, Touboul P, Turyshv SG, Anderson J, Tobar ME, Schmidt-Kaler F, Vigué J, Madej AA, Marmet L, Angonin M, Delva P, Tournenc P, Metris G, Müller H, Walsworth R, Lu ZH, Wang LJ, Bongs K, Toncelli A, Tonelli M, Dittus H, Lämmerzahl C, Galzerano G, Laporta P, Laskar J, Fienga A, Roques F, Sengstock K (2009) Quantum physics exploring gravity in the outer solar system: the SAGAS project. *Experimental Astronomy* 23:651–687, DOI 10.1007/s10686-008-9118-5, [arXiv:0711.0304\[gr-qc\]](#)
- Zarka P, Pedersen BM, Lecacheux A, Kaiser ML, Desch MD, Farrell WM, Kurth WS (1995) Radio emissions from Neptune. In: D P Cruikshank, M S Matthews, & A M Schumann (ed) *Neptune and Triton*, pp 341–387
- Zharkov V, et al (1978) Interior structure of the planets. in *Physics of Planetary Interiors*
- Zharkov VN, Gudkova TV (2010) Models, figures and gravitational moments of Jupiter’s satellite Io: Effects of the second order approximation. *Planetary and Space Science* 58:1381–1390, DOI 10.1016/j.pss.2010.06.004
- Zimmer C, Khurana KK, Kivelson MG (2000) Subsurface Oceans on Europa and Callisto: Constraints from Galileo Magnetometer Observations. *Icarus* 147:329–347, DOI 10.1006/icar.2000.6456